DYNAMICS AND NONLINEAR CONTROL OF ELECTROMAGNETIC DOCKING/ASSEMBLY AND PROXIMITY OPERATIONS

By

KE HUO

A THESIS PRESENTED TO THE GRADUATE SCHOOL
OF THE UNIVERSITY OF FLORIDA IN PARTIAL FULFILLMENT
OF THE REQUIREMENTS FOR THE DEGREE OF
MASTER OF SCIENCE

UNIVERSITY OF FLORIDA

2012

To my parents

ACKNOWLEDGMENTS

I would like take the time to publicly acknowledge and thank: committee members, Dr. Wiens, Carl D. Crane and Prabir Barooah, for all the feedbacks on my thesis, professors from class, Warren Dixon and Norman G. Fitz-Coy, for lecturing great on nonlinear control and dynamics respectively. I also want to thank Yiming Xu, Karl Brandt, Yilun Liu, Paul Moore, for the great supports. Of course, another person I should thank is my girlfriend who hasn't been appearing for last two years. Additionally thanks go out to all the help I have received in writing.

TABLE OF CONTENTS

LIST OF TABLES

LIST OF FIGURES

LIST OF SYMBOLS

A	The area enclosed by a coil loop
$\underline{A}$	Vector potential
$\underline{B}$	Magnetic field with unit of tesla (symbol T)
$\underline{E}$	Electric field with unit of V/m
$\underline{F}$	Force
$\underline{F}_{ex}$	External force
$\mathcal{F}^A$	Reference frame fixed on foil A
$\underline{F}_A$	Reaction force on current loop A
$\mathcal{F}^I$	The interial reference frame
$\mathcal{F}^o$	The orbit reference frame
$\mathcal{F}^R$	Rotated reference frame
$\underline{H}_o^A$	Angular momentum of body A about point o
i	Current through a coil
$\underline{J}$	Current density vector with unit of A/m
$\underline{J}_d$	Displacement current density vector
$\underline{l}$	Line segment of the coil
$\mathcal{L}_\infty$	The space of bounded sequences
$\underline{\mu}$	Magnetic dipole moment
m	Mass
m_A	Mass of body A

μ_0	Permeability of free space constant, $4\pi \times 10^{-6}$ N/A^{-2}
N	Number of turns in a coil
$\underline{\hat{n}}$	The unit vector along axis of coil loop
∇	Gradient operator
$\underline{\nabla}\cdot$	Divergence
$\underline{\nabla}\times$	Curl
$\underline{\omega}$	Angular velocity
${}^{C}\underline{\omega}_{A/B}$	Angular velocity of body A with respect to Frame B expressed in Frame C
$\underline{P}^{A}$	Linear momentum of body A
π	The ratio of a circle's circumference to its diameter
$R(x,\ \theta)$	Principal rotation matrix of angle θ about x axis
$R(y,\ \phi)$	Principal rotation matrix of angle ϕ about y axis
$R(z,\ \psi)$	Principal rotation matrix of angle ψ about z axis
$R_{A/B}$	Rotation matrix from Frame A to Frame B
$\underline{\tau}$	Torque about the center of a loop
$\underline{\tau}_A$	Torque about the center of a loop A
$\underline{\tau}_{ex}$	External torque
U	Potential energy
u	Control input signal
$\underline{u}$	Control input signal vector

V_L Lyapunov candidate function

$\underline{\hat{x}}$ Unit vector along x axis

$\underline{\hat{y}}$ Unit vector along y axis

$\underline{\hat{z}}$ Unit vector along z axis

Abstract of Thesis Presented to the Graduate School
of the University of Florida in Partial Fulfillment of the
Requirements for the Degree of Master of Science

DYNAMICS AND NONLINEAR CONTROL OF ELECTROMAGNETIC
DOCKING/ASSEMBLY AND PROXIMITY OPERATIONS

By

Ke Huo

August 2012

Chair: Gloria J. Wiens
Major: Aerospace Engineering

The use of electromagnetic actuators in attitude control system has been considered as an effective and reliable approach for low Earth orbit (LEO) satellites. One recent application is Electromagnetic Formation Flight (EMFF) which controls the relative translational degrees of freedom between satellites. Compared to the use of traditional thrusters, using an electromagnetic force and torque in multi-spacecrafts missions has some distinct advantages, such as no propellant consumption and plume contamination, as well as continuous controllability. The advantages of electromagnets however come at the cost of highly nonlinear and coupled dynamics. Extending the EMFF approach to rendezvous and docking, this paper focuses on providing small satellites a docking capability in both axial and circumferential directions through the use of two sets of electromagnetic coils. For implementation, a novel control strategy is also presented.

The first problem which needs to be solved is the model of electromagnetic field and generated force and torque between two electromagnetic coils. The force and torque are not only functionally related to the characteristics of the coils but are also dependent on the relative position and attitude of the two satellites in proximity of one another. Both a numerically exact model and an analytic far-field model have been built and compared in this paper.

This thesis provides a capable electromagnetic docking strategy for two satellites. Each of the satellites in electromagnetic docking system is equipped with reaction

wheels and a set of three orthogonal current driven coils. With the assistance of reaction wheels, decoupling the 3-dimensional docking problem to several steps of principal basic cases provides full docking capabilities of the small satellites. Dynamics analysis and nonlinear controller design have been developed. As well, an overall control strategy and a complete simulation have been demonstrated. Power consumption and disturbances due to both gravity and the earth magnetic field are considered in an on-orbit scenario.

CHAPTER 1
INTRODUCTION

1.1 Motivation

In general, autonomous rendezvous and docking technology includes two spacecrafts starting at a remote distance, coming together into a common orbit, rendezvous, docking and control of the new combined spacecraft [19]. Traditional use of this technology contains space exploration and supply and repair of vehicles [11]. Moreover, there has been a tendency in recent years to develop a spacecraft modular architecture design concept [14]. This concept expands application and needs of the docking technology more widely.

Proximity operations and docking are critical phases of a rendezvous and docking mission due to both translational and rotational maneuvers are required. Some critical issues due to use of traditional maneuvering techniques, such as a thruster based propellant system, are prone to plume impingement and the possibility of collision caused by the discontinuous propulsion [19].

Inspired by a common daily phenomenon that two magnets can adjust the relative position and attitude, and then achieve self-docking, the idea of introducing electromagnetic force and torque into docking/assembly and proximity operations is the approach of interest in this thesis. Compared to the use of thrusters, using an electromagnetic force and torque has some distinct advantages, such as no propellant consumption and plume contamination, as well as continuous controllability. The advantages of electromagnets however come at the cost of highly nonlinear and coupled dynamics.

This thesis starts from the idea of electromagnetic docking, provides a capable way to implement this idea in a scenario with fair assumptions, demonstrates a complete docking mission simulation in this scenario.

1.2 Previous Relative Work

The exploitation of the use of magnetic force and torque in space missions can be roughly categorized into the following three areas: using electromagnetic actuators proven to be an effective and reliable attitude control system for low Earth orbit (LEO) satellites [16]; the electromagnetic formation flight (EMFF) controls the relative translational degrees of freedom between satellites [15]; and electromagnetic docking/assembly considering both translational and rotational degrees of freedom [22, 23]. In the following paragraphs, previous work related to these three types of applications is introduced.

The electromagnetic actuators in an attitude control system operate on the basis of interaction between a set of three orthogonal current-driven magnetic coils and the geomagnetic field. These coils can therefore generate corresponding torques. These torques can either be used to dump angular momentum [2] or to actively control attitude. First, the magnetic control system is designed for use with some stabilization method such as spinning and bias momentum [17]. Then, in more recent decades, purely magnetic attitude control has been studied. Due to the low cost, flexible shaping, low energy consuming, simple hardware requirement for moderate attitude control of magnetic attitude control, magnetic actuators are preferred in small satellites and micro-satellites, as shown in Figure 1-1 [5].

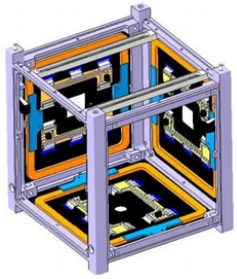

Figure 1-1. Magnetic actuator configuration in a CubeSat.

The concept of using electromagnetic force to provide the relative positioning control for satellites formation flight have been researched by two main groups: MIT

Space Systems Lab [15], and the University of Tokyo/ISAS [9]. The EMFF uses high temperature superconducting wire technology to generate the electromagnetic force to maintain and reconfigure the satellites formation [1]. The EMFF concentrates on translational degrees of freedom control. It is assumed that the torque and angular momentum generated during the operation will be absorbed by reaction wheels [15].

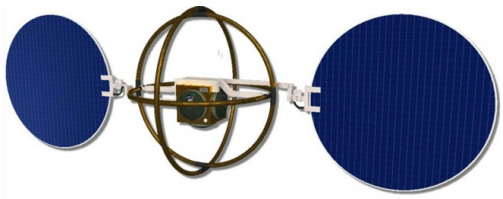

Figure 1-2. Electromagnetic formation flight vehicle.

Spacecraft electromagnetic docking technology is similar to the EMFF conception (Figure 1-2), yet the main difference between these two include, both translational and rotational control have to be concerned. Analogy of the daily magnets attraction phenomenon to docking problem is straightforward. A concept of self-docking capability of electromagnets presents that under some specific constraints for initial conditions, the relative position/attitude automatically decreasing to zero, not considering the docking velocity [22, 23]. Then, reference [22, 23] has constrained the docking problem to small relative attitude assumption. As well, the relative velocity is the only control objective. However, the linearization based on small relative attitude and coplanar assumption makes this paper insubstantial in some degree.

Based on the above, this thesis provides a feasible way to use electromagnetic in docking/assembly and proximity operation for small satellites under some fair assumptions. Not only the translational control but also the rotational control during the docking process has been investigated. Different from EMFF conception, the torques generated due to the misalignment of dipoles have been considered as the torque source for attitude adjustment, instead of been canceled by reaction wheels.

1.3 Overview of the Research and Thesis

Electromagnetic docking in this thesis is the idea of using sets of orthogonal current driven coils, coupled with reaction wheels, to provide the relative position and attitude control in docking mission. Notice that, the reaction wheels in this thesis are used only for stabilizing the satellite when the docking strategy needs, the torque generated by electromagnetic coils provide the control of relative attitude.

The docking strategy is designed to adjust the attitude and track a desired distance trajectory simultaneously, then maintain the adjusted relative attitude and track a desired approaching trajectory. The attitude adjustment has been decoupled to two steps, alignment of the dominant rings and twist adjustment of coils perpendicular to the dominant coil about the aligned co-axial. The Figure 1-3 demonstrates the docking strategy.

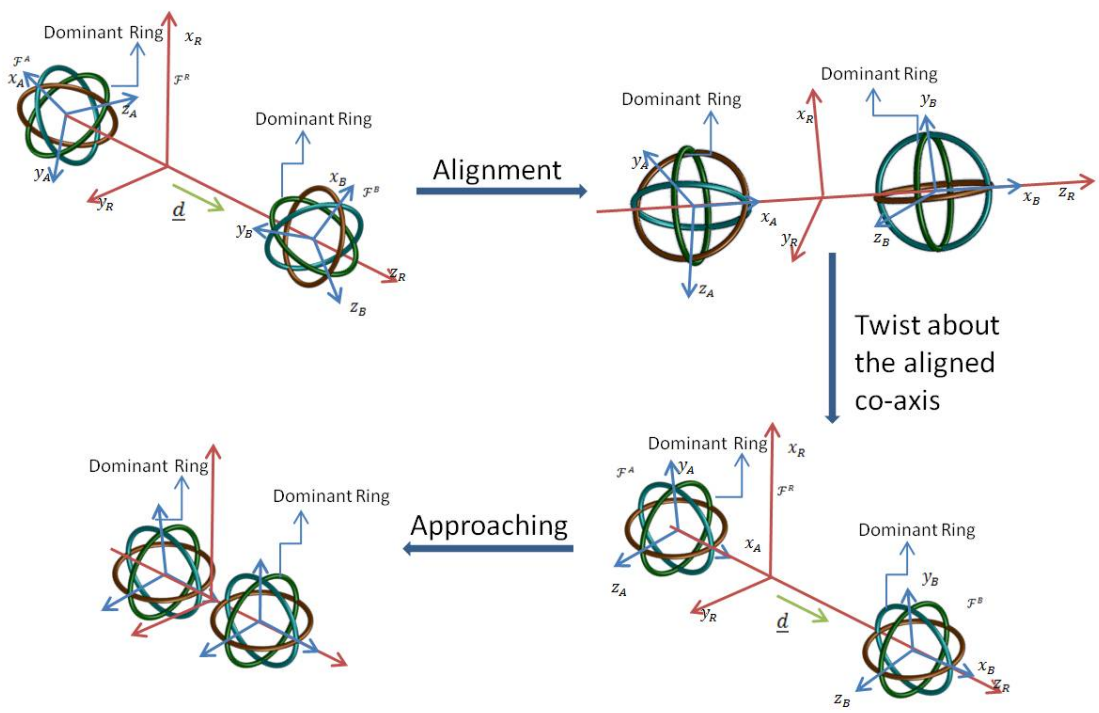

Figure 1-3. Electromagnetic docking strategy.

The electromagnetic docking has wide prospects of applications in the future:

- Orbit service could benefit from the improvement of continuous controllability and zero propellant consumption.
- Thinking about a series of modules equipped with electromagnetic docking system, each of them has a partial function. By docking together they might have ability to cooperate as a complete functional satellite.
- If a conceptual flying space robotics is designed to be manipulated by a set of coils equipped on the mother station, then the propulsion system and attitude control system of robotics could be diminished.
- Also, considering self-assembly architecture in the space, by using autonomous electromagnetic docking technology, only the main body needs full attitude control system and propulsion system.

The structure of this thesis is developed as such:

In Chapter 2, exact model and far field model of electromagnetic force and torque has been presented and compared. This chapter is the basis of derivation of dynamics equations.

In Chapter 3, details of the system description have been demonstrated, followed by the overall docking strategy introduction. Docking mission has been divided to several steps of principal basic cases. The development of dynamic models of principal basic cases constitutes the main body of this chapter.

In Chapter 4, control strategy and controller design for each step has been investigated. As well, simulation results of each controller are demonstrated and discussed. A complete simulation combined these controllers guided by the control strategy is presented.

In Chapter 5, challenges when this system is operating in LEO scenario have been shown. Difficulties and possible solutions have been discussed.

In Chapter 6, summary and main contributes of this thesis have been concluded. Some suggestions on future work also are included.

CHAPTER 2
MODELLING THE ELECTROMAGNETIC FORCES ADC TORQUES

2.1 Overview

In this thesis, the electromagnetic docking system consists of two satellites. Each satellite is equipped with one or more coils. To study the dynamics and derive the dynamics equations of this system, one must first develop the theoretical models of the magnetic field, forces and torques generated. Using the principle of magnetic field theory [13], the following sections describe the applicable theory. Based on this theory, the corresponding force and torque equations needed for generating the full dynamic model are presented. Chapter 3 will detail the corresponding dynamics equations.

2.2 Derivation of the Exact Model

2.2.1 Magnetic Field

The difference between electric field $\underline{E}$ and the magnetic field $\underline{B}$: electric charge is a point source of $\underline{E}$, while motion of charged particles, (i.e. current), is the source of $\underline{B}$. The literatures show that there are no experiments indicating existence of magnetic monopoles or magnetic charge, though searching for them continues to be an interesting challenge [13]. since a magnetic field does not have a point source, the divergence of the magnetic field must be zero, and can be expressed as:

$$\underline{\nabla} \cdot \underline{B} = \underline{0}\,, \tag{2–1}$$

where ∇ is the gradient operator, $\underline{\nabla} \cdot \underline{B} = \underline{0}$ is the divergence of $\underline{B}$.

The curl of magnetic field is given by Ampere's equation for magnetostatics, i.e. for the field from current distribution which is constant in time

$$\underline{\nabla} \times \underline{B} = \mu_0\, \underline{J}\,, \tag{2–2}$$

where $\underline{J}$ is the current density vector, and μ_0 is the permeability of free space. Equation (2–2) can also be modified as following for time variant problems.

$$\underline{\nabla} \times \underline{B} = \mu_0 \left(\underline{J} + \underline{J}_d \right) , \tag{2–3}$$

where $\underline{J}_d$ is displacement current density vector. In a laboratory system of charges and currents, the displacement current is normally very small compared to typical charge currents. To observe $\underline{J}_d$ experimentally requires high frequencies, large electric field, or both. Furthermore, the presumption that the magnetic fields and currents will vary slowly over time could be made, then magnetostatics can be assumed.

By introducing a vector potential $\underline{A}$, the electromagnetic field can be expressed as:

$$\underline{B} = \underline{\nabla} \times \underline{A} . \tag{2–4}$$

From reference [13], the general solution for $\underline{A}$ could be written as:

$$\underline{A}(s) = \frac{\mu_0}{4\,\pi} \iiint_{Vol} \frac{\underline{J}(\underline{\rho})}{|\underline{s} - \underline{\rho}|} \, \mathrm{d}^3 \, \underline{\rho} , \tag{2–5}$$

where $\underline{\rho}$ is the position vector of the element volume ($\mathrm{d}^3 \, \underline{\rho} = \mathrm{d}\rho_x \, \mathrm{d}\rho_y \, \mathrm{d}\rho_z$) within electrical conducting material, $\underline{s}$ is the position vector from the element volume to potential vector's location.

For a current loop, as shown in Figure 2-1, the wire is assumed to have negligible thickness, and the current density is zero everywhere but within the wire. The equation for the vector potential at location P can then be reduced to a path integral around the loop of current.

$$\underline{A}(\underline{s}) = \frac{\mu_0 \, N \, i}{4\,\pi} \oint \frac{1}{\|\underline{s} - \underline{a}\|} \, \mathrm{d}\underline{l} , \tag{2–6}$$

where N is the number of turns; i is the current, $\underline{s}$ is the vector from a small segment of the coil, $\mathrm{d}\underline{l}$, to point P, $\underline{a}$ is the radial position vector of segment $\mathrm{d}\underline{l}$ relative to the center of coil.

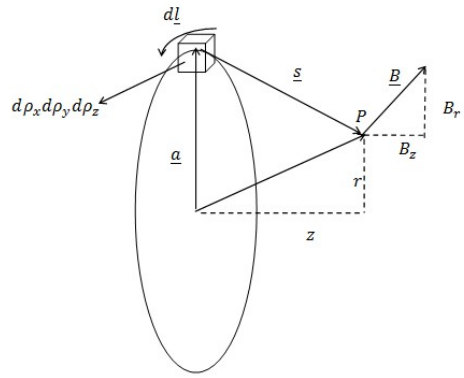

Figure 2-1. A loop of current.

Substituting into (2–6) to (2–4), the magnetic field can be expressed as:

$$\underline{B} = \underline{\nabla} \times \frac{\mu_0 N i}{4 \pi} \oint \frac{1}{\|\underline{s} - \underline{a}\|} \, \mathrm{d}\underline{l} \,. \tag{2–7}$$

Since the operation $\oint$ is based on $\underline{s}$, it can commute with integrand. Also, by using

$$\underline{\nabla} \times \frac{1}{\|\underline{s} - \underline{a}\|} = -\frac{\underline{s} - \underline{a}}{\|\underline{s} - \underline{a}\|^3} \,, \tag{2–8}$$

(2–7) gives

$$\underline{B} = \frac{\mu_0 N i}{4 \pi} \oint \frac{\underline{s} - \underline{a}}{\|\underline{s} - \underline{a}\|^3} \times \mathrm{d}\underline{l} \,. \tag{2–9}$$

Due to the difficulty of integrating the reciprocal of the square of magnitude of the $\|\underline{s} - \underline{a}\|^3$, solving for the magnetic field is not straightforward. As such, the magnetic field $\underline{B}$ can only be written analytically in terms of elliptical integrals when it is off axis. For the off axis case the magnetic field can be expressed in terms of radial and axial components as [4]:

$$\begin{aligned} \underline{B} = & \frac{\mu_0 N i}{2 \pi a} \frac{1}{\sqrt{Q}} \left[E(m) \frac{1 - \alpha_B^2 - \beta_B^2}{Q - 4 \alpha_B} + K(m) \right] \hat{\underline{z}} \\ & + \frac{\mu_0 N i}{2 \pi a} \frac{1}{\sqrt{Q}} \left[E(m) \frac{1 + \alpha_B^2 + \beta_B^2}{Q - 4 \alpha_B} - K(m) \right] \hat{\underline{r}} \,, \end{aligned} \tag{2–10}$$

where $E(m)$ is the first kind of elliptical integral, and $K(m)$ is the second kind of elliptical integral, and

$$\alpha_B = \frac{r}{a}\,, \quad \beta_B = \frac{z}{a}\,, \quad \gamma_B = \frac{z}{r}\,, \quad Q_B = (1+\alpha_B)^2 + \beta_B^2\,, \quad m_B = \sqrt{\frac{4\,\alpha_B}{Q_B}}\,. \tag{2–11}$$

2.2.2 Force and Torque

In this section, the force and torque are derived so that one may model the interaction behavior between of the two satellites. Figure 2-2 illustrates the fundamental configuration of the coils each represents a satellite.

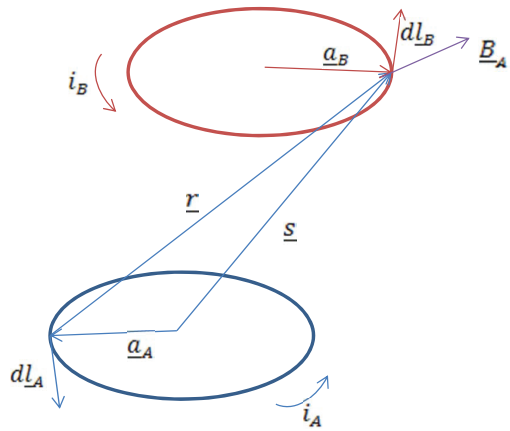

Figure 2-2. Two loops of current.

When a wire carrying an electrical current is placed in a magnetic field, each moving charges, experiences he Lorentz force. By using Lorentz force law, for each small segment of wire $\mathrm{d}\underline{l}$ carrying current i, the force acting on this segment is given by:

$$\mathrm{d}\underline{F} = i\,\mathrm{d}\underline{l} \times \underline{B}\,. \tag{2–12}$$

Integrating (2–12) over the length of the wire, total electromagnetic force on the wire is given by:

$$\underline{F} = i \int \mathrm{d}\underline{l} \times \underline{B}\,, \tag{2–13}$$

Applying this equation to the case illustrated in Figure 2-2, the force acting on the second loop of current is:

$$\underline{F}_B = i_B \int \mathrm{d}\underline{l}_B \times \underline{B}_A \,, \tag{2–14}$$

in which $\underline{B}_A$ is the electromagnetic field at position of $\mathrm{d}\underline{l}_B$ created by loop A.

The reaction force acts on current loop A is of course:

$$\underline{F}_A = -\underline{F}_B = -i_B \int \mathrm{d}\underline{l}_B \times \underline{B}_A \,. \tag{2–15}$$

The torque on loop B about the center of the loop due to incremental force $\mathrm{d}\underline{F}_B$ is given by:

$$\underline{\tau}_B = \int \underline{a}_B \times \mathrm{d}\underline{F}_B \,. \tag{2–16}$$

Combining the above equations with the field results in Section 2.2.1, the equations for both force and torque have double integrals, which limits the ability to solve them analytically. Consequently, insights about the force and torque model are hard to determine. Therefore, to obtain approximations that can be derived analytically, simplification and linearisation by using Taylor series will be used in the following section.

2.3 Far-Field Model of Electromagnetic Force and Torque

2.3.1 Derivation of Far-Field Model

At a sufficiently large distance, the magnetic field generated by a current loop behaves as a magnetic dipole when it comes to a sufficient large distance. Hence, a current loop could be visualized as a bar magnet aligned with the axis of the loop pointing in the direction given by right hand rule.

To analytically express this behavior, the force and torque expression contains $\|\underline{s} - \underline{a}\|$ term in the dominator. When large distance assumption is made, we can simplify the model due to

$$\|\underline{a}\| \ll \|\underline{s}\| \,. \tag{2–17}$$

Expand $1/\|\underline{s}-\underline{a}\|$ about $a/s \approx 0$ using Taylor series yields

$$\frac{1}{\|\underline{s}-\underline{a}\|} = \frac{1}{s} + \frac{\underline{s}\cdot\underline{a}}{s^3} + \text{H.O.T}\,, \tag{2–18}$$

where $\underline{s}\cdot\underline{a}$ is dot product of vectors $\underline{s}$ and $\underline{a}$, and H.O.T are the higher order terms that are approximated to be zero.

Substituting (2–18) into (2–5) and (2–6) for the magnetic vector potential, and observing the first term with $1/s$ integrates to zero, then:

$$\underline{A}(\underline{s}) = \frac{\mu_0}{4\,\pi}\iiint\left(\frac{1}{s}+\frac{\underline{s}\cdot\underline{a}}{s^3}\right)\underline{J}(\underline{\rho})\,\mathrm{d}^3\underline{\rho} = \frac{\mu_0}{4\,\pi}\iiint\frac{\underline{s}\cdot\underline{a}}{s^3}\,\underline{J}(\underline{\rho})\,\mathrm{d}^3\underline{\rho}\,, \tag{2–19}$$

$$\text{and}\quad \underline{A}(\underline{s}) = \frac{\mu_0\,N\,i}{4\,\pi}\oint\left(\frac{1}{s}+\frac{\underline{s}\cdot\underline{a}}{s^3}\right)\mathrm{d}\underline{l} = \frac{\mu_0\,N\,i}{4\,\pi\,s^3}\oint(\underline{s}\cdot\underline{a})\,\mathrm{d}\underline{l}\,. \tag{2–20}$$

Using vector calculus, it has been proven in reference [13], the integral in (2–19) and (2–20) can be rewritten as:

$$\iiint\frac{\underline{s}\cdot\underline{\rho}}{s^3}\,\underline{J}(\underline{\rho})\,\mathrm{d}^3\underline{\rho} = \underline{\mu}\times\underline{s}\,, \tag{2–21}$$

$$N\,i\oint\underline{s}\cdot\underline{a}\,\mathrm{d}\underline{l} = \underline{\mu}\times\underline{s}\,, \tag{2–22}$$

in which $\underline{\mu}$ is called magnetic dipole moment:

$$\underline{\mu} = \frac{1}{2}\iiint\underline{\rho}\times\underline{J}(\underline{\rho})\,\mathrm{d}^3\underline{\rho}\,. \tag{2–23}$$

Substitute back to (2–21), the vector potential of a magnetic dipole can be expressed as:

$$\underline{A}(\underline{s}) = \frac{\mu_0}{4\,\pi}\frac{\underline{\mu}\times\underline{s}}{s^3}\,. \tag{2–24}$$

For a current loop, the magnetic dipole moment is:

$$\underline{\mu} = N\,i\oint\frac{1}{2}\,\underline{a}\times\mathrm{d}\underline{l} = N\,i\,A\,\underline{\hat{n}}\,, \tag{2–25}$$

where N is the number of turns, i is the current, A is the area enclosed by the loop, and $\underline{\hat{n}}$ is the vector along the axis of the loop. The corresponding magnetic field

mathematical expression then takes the form:

$$\underline{B} = \underline{\nabla} \times \underline{A} = \frac{\mu_0}{4\,\pi}\,\underline{\nabla} \times (\frac{\underline{\mu} \times \underline{s}}{s^3})\,, \tag{2–26}$$

Using the properties of the gradient operator ($\underline{\nabla}$)

$$\underline{\nabla} \times (\underline{u} \times \underline{v}) = \underline{u}\,(\underline{\nabla} \cdot \underline{v}) - \underline{v}\,(\underline{\nabla} \cdot \underline{u}) + (\underline{v} \cdot \underline{\nabla})\,\underline{u} - (\underline{u} \cdot \underline{\nabla})\,\underline{v}\,, \tag{2–27}$$

yields

$$\underline{\nabla} \times (\frac{\underline{\mu} \times \underline{s}}{s^3}) = \underline{\mu}\,(\underline{\nabla} \cdot \frac{\underline{s}}{s^3}) - \frac{\underline{s}}{s^3}\,(\underline{\nabla} \cdot \underline{\mu}) + (\frac{\underline{s}}{s^3} \cdot \underline{\nabla})\,\underline{\mu} - (\underline{\mu} \cdot \underline{\nabla})\,\frac{\underline{s}}{s^3}\,. \tag{2–28}$$

Since $\underline{\mu}$ is not a function of s, then $\underline{\nabla} \cdot \underline{\mu} \equiv 0$ and $(\frac{\underline{s}}{s^3} \cdot \underline{\nabla})\underline{\mu} \equiv \underline{0}$. Therefore,

$$\begin{aligned}
\underline{\nabla} \cdot \frac{\underline{s}}{s^3} &= \frac{\partial}{\partial x}\left(\frac{x}{s^3}\right) + \frac{\partial}{\partial y}\left(\frac{y}{s^3}\right) + \frac{\partial}{\partial z}\left(\frac{z}{s^3}\right) \\
&= \left(\frac{1}{s^3} - \frac{3}{x^5}\,x^2\right) + \left(\frac{1}{s^3} - \frac{3}{x^5}\,y^2\right) + \left(\frac{1}{s^3} - \frac{3}{x^5}\,z^2\right) \\
&= 0\,,
\end{aligned} \tag{2–29}$$

$$\begin{aligned}
(\underline{\mu} \cdot \nabla)\,\frac{\underline{s}}{s^3} &= \mu_x\,\frac{\partial}{\partial x}\left(\frac{x}{s^3}\right) + \mu_y\,\frac{\partial}{\partial y}\left(\frac{y}{s^3}\right) + \mu_z\,\frac{\partial}{\partial z}\left(\frac{z}{s^3}\right) \\
&= \mu_x\,\left(\frac{\underline{\hat{e}}_x}{s^3} - \frac{3}{s^5}\,x\,\underline{s}\right) + \mu_y\,\left(\frac{\underline{\hat{e}}_y}{s^3} - \frac{3}{s^5}\,y\,\underline{s}\right) + \mu_z\,\left(\frac{\underline{\hat{e}}_z}{s^3} - \frac{3}{s^5}\,z\,\underline{s}\right) \\
&= \frac{1}{s^3}\,\underline{\mu} - \frac{3\,\underline{s}}{s^5}\,(\underline{s} \cdot \underline{\mu})\,.
\end{aligned} \tag{2–30}$$

Finally, we have:

$$\underline{B} = \frac{\mu_0}{4\,\pi}\left(\frac{3\,\underline{s}\,(\underline{s} \cdot \underline{\mu})}{s^5} - \frac{\underline{\mu}}{s^3}\right) = \underline{B}(\underline{s}, \underline{\mu})\,, \tag{2–31}$$

which varies in $\underline{s}$ and $\underline{\mu}$).

For the far-field approximation $\underline{s} \approx \underline{a}$. Hence, the potential energy of a magnetic dipole of coil B in a magnetic field of coil A ($\underline{B}_A(\underline{d})$ is given by:

$$U(\underline{d}) = -\underline{\mu}_B \cdot \underline{B}_A(\underline{d})\,, \tag{2–32}$$

where $\underline{d}$ is the vector connecting the center of dipole A to dipole B, $\underline{B}_A(\underline{d})$ is the approximation of $\underline{B}_A(\underline{s})$, and $\underline{\mu}_B$ is magnetic moment due to coil B. The force on dipole

B is simply derived from the gradient of the potential energy.

$$\underline{F}_B = -\nabla U = \nabla(\underline{\mu}_B \cdot \underline{B}_A) = \frac{\mu_0}{4\,\pi}\,\nabla\left(\frac{3\,(\underline{\mu}_B \cdot \underline{d})\,(\underline{d} \cdot \underline{\mu}_A)}{d^5} - \frac{\underline{\mu}_B \cdot \underline{\mu}_A}{d^3}\right) . \tag{2–33}$$

Again, noting $\underline{\mu}_A$ and $\underline{\mu}_B$ are not functions of d, therefore $\nabla\underline{\mu}_A = 0$, $\nabla\underline{\mu}_B = 0$. Similar to the above derivation, (2–33) results in

$$\underline{F}_B = -\frac{3\,\mu_0}{4\,\pi}\left(-(\underline{\mu}_A \cdot \underline{\mu}_B)\,\frac{\underline{d}}{d^5} - (\underline{\mu}_A \cdot \underline{d})\,\frac{\underline{\mu}_B}{d^5} - (\underline{d} \cdot \underline{\mu}_B)\,\frac{\underline{\mu}_A}{d^5} + 5\,(\underline{\mu}_A \cdot \underline{d})\,(\underline{d} \cdot \underline{\mu}_B)\,\frac{\underline{d}}{d^7}\right) . \tag{2–34}$$

A torque applied over a rotation is equal to the change in potential energy.

$$\mathrm{d}U = -\underline{\tau} \cdot \mathrm{d}\underline{\theta} = -\mathrm{d}\underline{\mu} \cdot \underline{B}\,, \tag{2–35}$$

where

$$\mathrm{d}\underline{\mu} = \mathrm{d}\underline{\theta} \times \underline{\mu}\,. \tag{2–36}$$

Then,

$$-\,\underline{\tau} \cdot \mathrm{d}\underline{\theta} = -(\mathrm{d}\underline{\theta} \times \underline{\mu}) \cdot \underline{B} = -(\underline{\mu} \times \underline{B}) \cdot \mathrm{d}\underline{\theta}\,, \tag{2–37}$$

and

$$\underline{\tau}_B = \underline{\mu}_B \times \underline{B}_A\,. \tag{2–38}$$

Substituting,

$$\underline{\tau}_B = \frac{\mu_0}{4\,\pi}\left(\underline{\mu}_B \times \left(3\,(\underline{\mu}_A \cdot \underline{d})\,\frac{\underline{d}}{d^5} - \frac{\underline{\mu}_A}{d^3}\right)\right) . \tag{2–39}$$

By using Newton's third law, we have:

$$\underline{F}_A = -\underline{F}_B\,. \tag{2–40}$$

Note: $\underline{F}_A$ could have been derived using

$$\underline{F}_A = -\nabla U = \nabla(\underline{\mu}_A \cdot \underline{B}_B)\,, \tag{2–41}$$

which yields the same expression as (2–40).

Due to the conservation of angular momentum: since there are no external force and torque acted on this system, the total angular momentum should be zero:

$$\underline{\tau}_A + \underline{\tau}_B + \underline{d} \times \underline{F}_B = \underline{0}\,. \tag{2–42}$$

Therefore, we can determine torque acting on loop A:

$$\underline{\tau}_A = -\underline{\tau}_B - \underline{d} \times \underline{F}_B\,. \tag{2–43}$$

The above completes the derivation of the forces and torques in the vector far-field model between two currents loops. The analysis of the dynamics of this system detailed in Chapter 3 is based on this model. The dynamics can be described for two cases: 2 dimensional (2-D) coplanar, co-axial twist. These two special cases will leverage for achieving orientation and position control of two satellites which in general could be uncontrollable in at least one degree of freedom. The following sections, 2.3.2 through 2.3.4, provide representations of force and torque for three different cases. The concise form and computational convenience of this model will shown as well.

2.3.2 2 Dimensional (2-D) Coplanar Case

In the 2-D coplanar case, two current loops A and B are restricted to a plane as showing in Figure 2-3. The xz coordinate system is inertial coordinate system, $\mathcal{F}^I$; $x_A z_A$ and $x_B z_B$ are body fixed coordinate systems $\mathcal{F}^A$ and $\mathcal{F}^B$, coil A and coil B respectively; and $x_R z_R$ is rotated reference coordinate system, $\mathcal{F}^R$. For computing convenience, the force and torque is derived in the $\mathcal{F}^R$ frame.

Referring to Figure 2-3, the dipole moment vector of coil A and B (aligned with axes x_A and x_B, respectively) are first aligned with x_R, then rotate $(\alpha - \pi/2)$ and $(\beta - \pi/2)$ respectively about y_R.

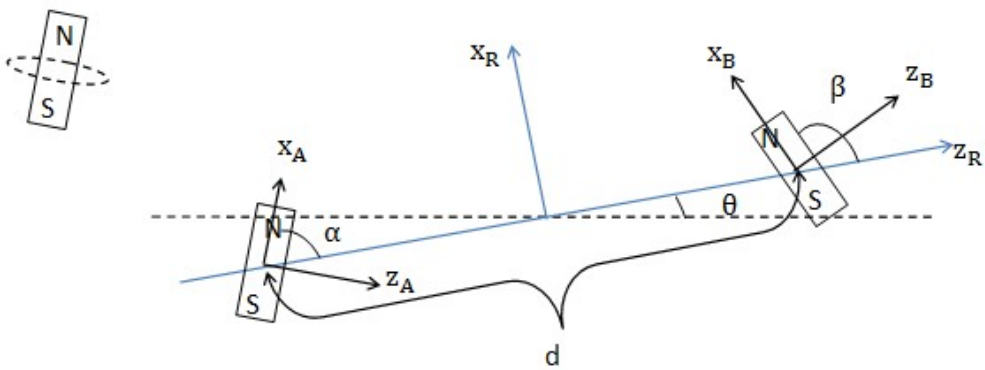

Figure 2-3. 2 dimensional (2-D) coplanar coils.

In $\mathcal{F}^R$, the dipole moment can be represented as:

$$ {}^R\underline{\mu}_A = \mu_A \sin\alpha\, \hat{\underline{x}}_R + \mu_A \cos\alpha\, \hat{\underline{z}}_R \,, \tag{2–44} $$

$$ {}^R\underline{\mu}_B = \mu_B \sin\beta\, \hat{\underline{x}}_R + \mu_B \cos\beta\, \hat{\underline{z}}_R \,, \tag{2–45} $$

$$ {}^R\underline{d} = \underline{d}\, \hat{\underline{z}}_R \,. \tag{2–46} $$

Substituting (2–46) into (2–34), (2–40), (2–39) and (2–43) results in following interaction forces and torques acting on the two coils in the rotated reference coordinate system, $\mathcal{F}^R$.

$$ \begin{aligned} \underline{F}_A = \frac{3\,\mu_0}{4\,\pi}\,\frac{\mu_A\,\mu_B}{d^4}\,\big(-(\cos\alpha\sin\beta + \cos\beta\sin\alpha)\,\hat{\underline{x}}_R \\ + (2\cos\alpha\cos\beta - \sin\beta\sin\alpha)\,\hat{\underline{z}}_R\big)\,, \end{aligned} \tag{2–47} $$

$$ \begin{aligned} \underline{F}_B = -\frac{3\,\mu_0}{4\,\pi}\,\frac{\mu_A\,\mu_B}{d^4}\,\big(-(\cos\alpha\sin\beta + \cos\beta\sin\alpha)\,\hat{\underline{x}}_R \\ + (2\cos\alpha\cos\beta - \sin\beta\sin\alpha)\,\hat{\underline{z}}_R\big)\,, \end{aligned} \tag{2–48} $$

$$ \underline{\tau}_A = -\frac{\mu_0}{4\,\pi}\,\frac{\mu_A\,\mu_B}{d^3}\,(2\sin\alpha\cos\beta + \cos\beta\sin\alpha)\,\hat{\underline{y}}_R\,, \tag{2–49} $$

$$ \underline{\tau}_B = -\frac{\mu_0}{4\,\pi}\,\frac{\mu_A\,\mu_B}{d^3}\,(2\cos\alpha\sin\beta + \sin\beta\cos\alpha)\,\hat{\underline{y}}_R\,. \tag{2–50} $$

From the above force and torque equations, one can observe some intuitive properties of two dipoles. As Figure 2-4 shows, when α and β are zero, the force is only

along with the z_R axis, as well the torque becomes to be zero. I.e. attraction or repulsive forces are present when the two coils are perfectly aligned. In this configuration, force and torque equations reduce to be:

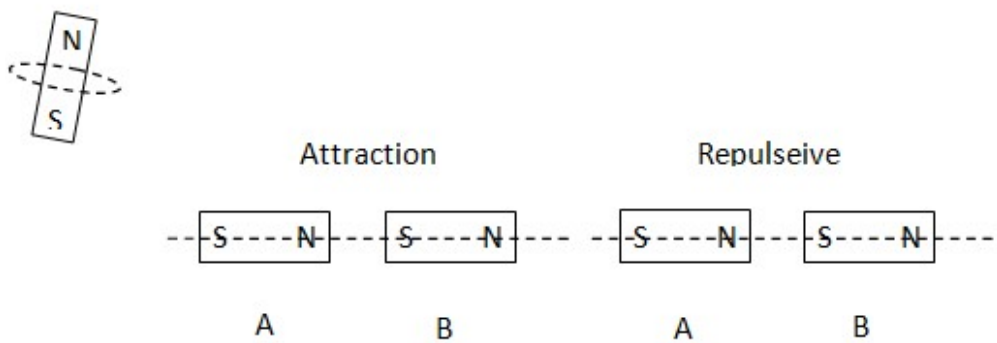

Figure 2-4. Aligned configuration.

$$\underline{F}_A = \frac{3\,\mu_0}{4\,\pi}\,\frac{\mu_A\,\mu_B}{d^4}\,\hat{\underline{z}}_R\,, \quad \underline{F}_B = -\frac{3\,\mu_0}{4\,\pi}\,\frac{\mu_A\,\mu_B}{d^4}\,\hat{\underline{z}}_R\,, \quad \underline{\tau}_A = \underline{\tau}_B = \underline{0}\,. \tag{2–51}$$

As Figure 2-5 shows, there are a set of lines due to the intersection of the $\underline{\tau}_A$ surface with the zero plane. Notice that for computational convenience, the factor $\frac{\mu_0\,\mu_A\,\mu_B}{4\,\pi\,d^3}$ has been normalized as 1. These lines correspond to the values of α and β for when the controllability of $\underline{\tau}_A$ vanishes. Similar situation will occur for $\underline{\tau}_B$. Observing the intersection lines in Figure 2-6, it is found that the control is lost simultaneously for both $\underline{\tau}_A$ and $\underline{\tau}_B$ at

$$\begin{aligned}(\alpha,\beta) =& \{\ldots,(-\pi,\pi),(0,0),(\pi,-\pi),\ldots\}\,,\\ & \{\ldots,(-\pi/2,-\pi/2),(\pi/2,-\pi/2),(\pi/2,\pi/2),\ldots\}\,,\\ \text{and}& \{\ldots,(-\pi,0),(\pi,0),(0,-\pi),\ldots\}\,.\end{aligned}$$

2.3.3 Co-Axial Twist Case

In co-axial case, two current loops C and D are restricted to be co-axial in z_R as shown in Figure 2-7. The $x_R z_R$ coordinate system is rotated reference coordinate

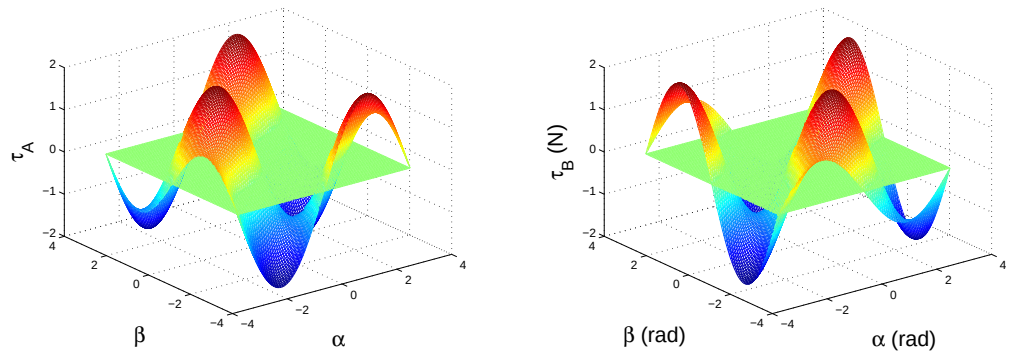

A Torque acting on coil A B Torque acting on coil B

Figure 2-5. Torques vary with angles.

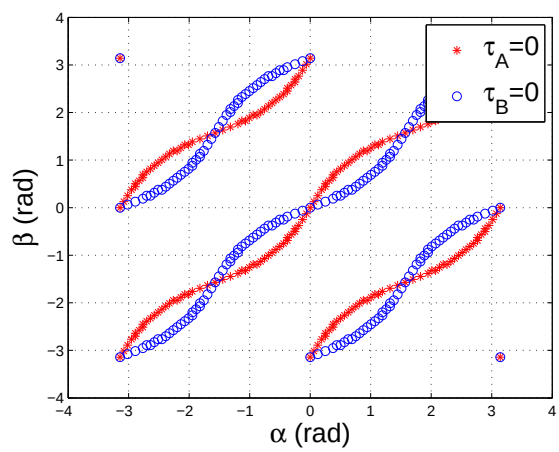

Figure 2-6. Intersecting lines for control lost for torques.

system, $\mathcal{F}^R$. Refer to Figure 2-7, dipole moment vectors of coil C and D (always aligned with x_C and x_D, respectively) are first aligned with x_R. Then rotate γ and δ respectively about z_R. When the two angles are zeros, the coils C and D are in the $y_R z_R$ plane.

The following mathematical expressions represent dipole moments in $\mathcal{F}^R$:

$$ {}^R\underline{\mu}_C = \mu_C \cos\gamma\, \hat{\underline{x}}_R + \mu_C \sin\gamma\, \hat{\underline{y}}_R \,, \tag{2–52} $$

$$ {}^R\underline{\mu}_D = \mu_D \cos\delta\, \hat{\underline{x}}_R + \mu_D \sin\delta\, \hat{\underline{y}}_R \,, \tag{2–53} $$

$$ {}^R\underline{d} = d\, \hat{\underline{z}}_R \,. \tag{2–54} $$

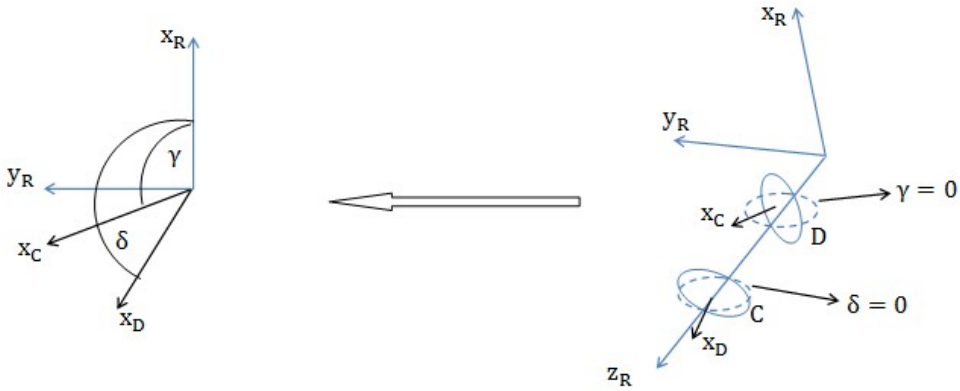

Figure 2-7. Co-axial twist case.

Substitute to (2–34), (2–40), (2–39) and (2–43), we have:

$$\underline{F}_C = \frac{3\,\mu_0\,\mu_c\,\mu_D}{4\,\pi\,d^4}\cos(\gamma-\delta)\,\hat{\underline{z}}_R\,, \tag{2–55}$$

$$\underline{F}_D = -\frac{3\,\mu_0\,\mu_c\,\mu_D}{4\,\pi\,d^4}\cos(\gamma-\delta)\,\hat{\underline{z}}_R\,, \tag{2–56}$$

$$\underline{\tau}_C = -\frac{\mu_0\,\mu_c\,\mu_D}{4\,\pi\,d^3}\sin(\gamma-\delta)\,\hat{\underline{z}}_R\,, \tag{2–57}$$

$$\underline{\tau}_D = \frac{\mu_0\,\mu_c\,\mu_D}{4\,\pi\,d^3}\sin(\gamma-\delta)\,\hat{\underline{z}}_R\,, \tag{2–58}$$

Some properties of the force and torque in this case can be concluded. First, forces are only on the $\hat{\underline{z}}_R$ axis. This means that once two coils enter the co-axial configuration, they would stay in this configuration. Second, torques are functions of $\mu_c\,\mu_D$ and $(\delta-\gamma)$. System would lose control of torque when $\delta-\gamma=0,\pi$ happens. However, this situation in general satisfies docking requirements of alignment (either N,N or N,S aligned). More details about this singularity will be shown in Chapter 3.

2.3.4 3 Dimensional (3-D) Representation

In this section the Euler Angle are used which are known for their intuitiveness to represent the rotation from rotated reference coordinate system $\mathcal{F}^R$ to body fixed coordinate system, $\mathcal{F}^A$ and $\mathcal{F}^B$. 3-2-1 sequence rotation will be used.

Referring to Figure 2-8, the dipole moment vectors of coil A and B (which are always aligned with x_A and x_B) are initially aligned with z_R, then rotate γ and δ respectively about z_R, following by rotating $(\alpha - \pi/2)$ about body fixed axis y_A and $(\beta - \pi/2)$ about body fixed axis y_B. Since the axial symmetry of rings, the last rotations about x_A and x_B do not affect the force and torque calculation.

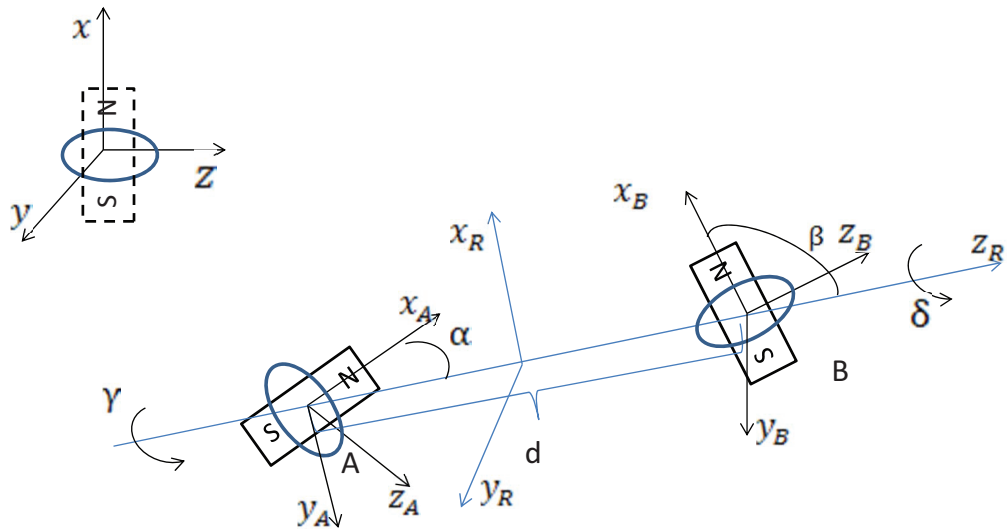

Figure 2-8. Euler angle representation.

The direct cosine matrix represents the transformation from $\mathcal{F}^R$ to $\mathcal{F}^A$, could be written as product of two principle rotation matrices:

$$
\begin{aligned}
R_{R/A} &= R_2(\alpha - \frac{\pi}{2})\, R_3(\gamma) \\
&= \begin{bmatrix} \sin\alpha & 0 & \cos\alpha \\ 0 & 1 & 0 \\ -\cos\alpha & 0 & \sin\alpha \end{bmatrix} \begin{bmatrix} \cos\gamma & \sin\gamma & 0 \\ -\sin\gamma & \cos\gamma & 0 \\ 0 & 0 & 1 \end{bmatrix} \\
&= \begin{bmatrix} \sin\alpha\cos\gamma & \sin\alpha\sin\gamma & \cos\alpha \\ -\sin\gamma & \cos\gamma & 0 \\ -\cos\alpha\cos\gamma & -\cos\alpha\sin\gamma & \sin\alpha \end{bmatrix}.
\end{aligned}
\tag{2–59}
$$

In $\mathcal{F}^R$, dipole moment vector of ring A could be described as:

$$
\begin{aligned}
{}^R\underline{\mu}_A &= R_{R/A}\,{}^A\underline{\mu}_A \\
&= \begin{bmatrix} \sin\alpha\cos\gamma & \sin\alpha\sin\gamma & \cos\alpha \\ -\sin\gamma & \cos\gamma & 0 \\ -\cos\alpha\cos\gamma & -\cos\alpha\sin\gamma & \sin\alpha \end{bmatrix} \begin{bmatrix} \mu_A \\ 0 \\ 0 \end{bmatrix} \\
&= \mu_A \begin{bmatrix} \sin\alpha\cos\gamma \\ \sin\alpha\sin\gamma \\ \cos\alpha \end{bmatrix}.
\end{aligned} \tag{2–60}
$$

Similarly, we can derive ${}^R\underline{\mu}_B$ out easily.

$$
{}^R\underline{\mu}_B = \mu_B \begin{bmatrix} \sin\beta\cos\delta \\ \sin\beta\sin\delta \\ \cos\beta \end{bmatrix}. \tag{2–61}
$$

Also,

$$
{}^R\underline{d} = \begin{bmatrix} 0 \\ 0 \\ d \end{bmatrix}. \tag{2–62}
$$

Substitute (2–60), (2–61) and(2–62) to (2–34) and (2–39), we have force and torque act on ring B represented in reference frame:

$$
{}^R\underline{F}_B = \frac{3\,\mu_0\,\mu_A\,\mu_B}{4\,\pi\,d^4} \begin{bmatrix} \cos\alpha\sin\beta\cos\delta + \sin\alpha\cos\beta\cos\gamma \\ \cos\alpha\sin\beta\sin\delta + \sin\alpha\cos\beta\sin\gamma \\ \sin\alpha\sin\beta\cos(\gamma-\delta) - 2\cos\alpha\cos\beta \end{bmatrix}, \tag{2–63}
$$

$$
{}^R\underline{\tau}_B = \frac{\mu_0\,\mu_A\,\mu_B}{4\,\pi\,d^3} \begin{bmatrix} \sin\alpha\cos\beta\sin\gamma + 2\cos\alpha\sin\beta\sin\delta \\ -\sin\alpha\cos\beta\cos\gamma + 2\cos\alpha\sin\beta\cos\delta \\ -\sin\alpha\sin\beta\sin(\gamma-\delta) \end{bmatrix}. \tag{2–64}
$$

2.3.5 Dipole Linear Superposition

Without loss of generality, assume satellite A and B are equipped by three orthogonal current rings, then the electromagnetic forces acting on rings equipped on satellite B could be calculated by summing up the forces due to the magnetic field generated by each ring on satellite A.

$$\underline{F}_B = \sum_{j=1}^{3} \sum_{i=1}^{3} \underline{f}_{ij} \,, \tag{2–65}$$

where $\underline{f}_{ij}$ is the force acting on j-th ring on satellite B due to the field generated by i-th ring on satellite A. Figure 2-9 shows the linear superposition

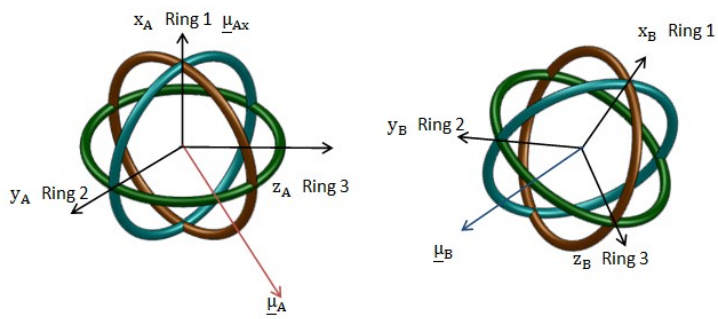

Figure 2-9. Linear superposition.

Notice, that the far-field model for force and torque is linear function of the magnetic dipole moments. Therefore, three orthogonal dipoles could be considered as a set of basis of a $\mathbb{R}^3$ space. That means, one can consider combination of these three dipole vectors as a new dipole vector. By changing the dipole moment of each of orthogonal rings, we have the ability to control both the direction and magnitude of the overall dipole vector.

$$\underline{\mu} = \sum_{i=1}^{3} \underline{\mu}_i \,. \tag{2–66}$$

The linear superposition simplifies the dynamic model when it involves multi-rings per satellite.

2.4 Model Evaluation

To verify the suitability of the above approximations used in modelling, the forces and torques of the far-field model and exact model are compared. Figure 2-10 presents the percentage error of magnitude with the coils in different configurations. Figure 2-11 presents the results for torque.

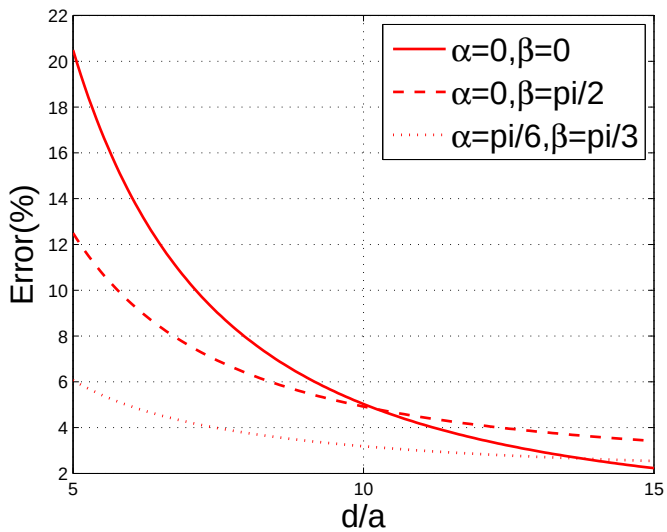

Figure 2-10. Comparing the far-field force model against the exact model.

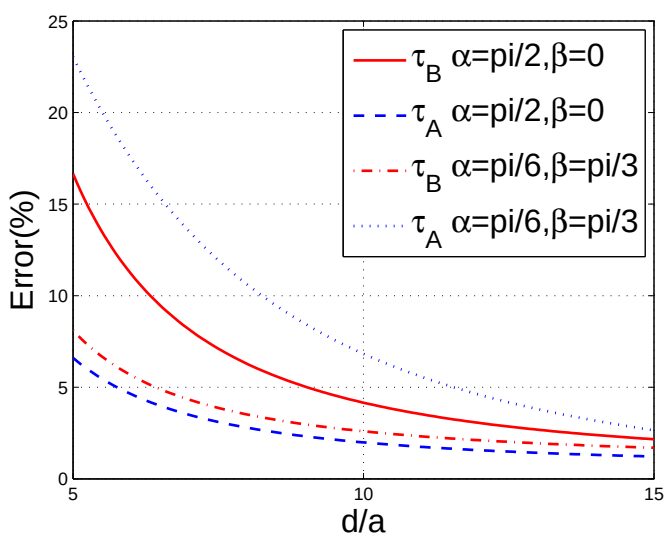

Figure 2-11. Comparing the far-field torque model against the exact model.

Usually, we admit a model is valid when the percentage error is less than 10%. From the two figures, we can see the error varies with different configuration of coils. Yet, overall, when distance is above approximately 6 times of the coil radii, error stays less than 10%.

CHAPTER 3
DYNAMIC MODELS

3.1 Overview

The purpose of this chapter is to develop system models. These models will be used for simulating and controller design. This chapter will starts off with system description as well as the overall docking strategy. Specifically, 3-D docking/operation problem will be decoupled to be several steps of principal basic cases, such as 2-D co-planar single coil case and co-axial twist single coil case. Next, the general rigid body dynamic modeling procedure will be presented. Then, development of dynamic models of principal basic cases constitutes the main body of this chapter. In the next chapter, the open loop behaviors of these cases, and subsequent controllers design for the principal basic cases, will be investigated. The overall control scheme will also be described, detailing how the resulting controller is implementable.

3.2 System Description

The electromagnetic docking/proximity operation system in this thesis typically involves two cooperative entities such as satellites, spacecrafts or assembly parts in space. Each of them will be equipped with three orthogonal current loops. Focusing on the dynamics and control problem of this system, the docking/operation/assembly will be simplified as follows into sequential operational steps: Step 1, adjust the attitude and maintain a constant distance or track a desired trajectory firstly; and Step 2, maintain the adjusted relative attitude and track a desired approaching trajectory.

3.2.1 Geometry of Different Coordinate System

Since orbital dynamics is not the primary objective in this thesis, several simplifications will be made here. Consequently, the definitions of coordinate system might be slightly different from common uses.

Inertial frame $\mathcal{F}^I$ is set to be the ECI reference frame which has its origin at the center of the Earth, one axis aalined with north pole, one points to vernal equinox, and

the third one completes a right handed axis system. Orbit frame $\mathcal{F}^o$ is defined as such, its origin is same as ECI frame's, one axis points towards the orbital plane normal, one axis aligned with the semi-major axis of the obit, the third one completes a right handed axis system. The $\mathcal{F}^A$ and $\mathcal{F}^B$ are defined as body fixed coordinate system to represent the orientations of satellite A and B. Figure 3-1 illustrates these definitions. Without losing generality, set $\mathcal{F}^I = \mathcal{F}^o$, showed as right part of Figure 3-1. For the convenience of electromagnetic force and torque representation, $\mathcal{F}^R$ is defined as rotated reference coordinate system, in which z_R axis is aligned with distance vector $\underline{d}$ points from origin of $\mathcal{F}^A$ to origin of $\mathcal{F}^B$, as shown in Figure 3-2. Origin of $\mathcal{F}^R$ is at the center of mass of the system of two satellites.

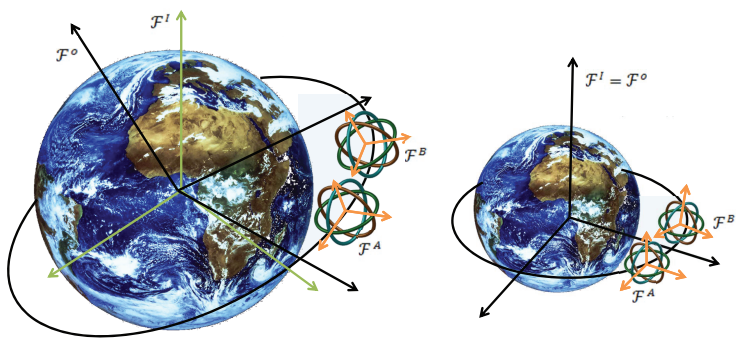

Figure 3-1. Geometry of different coordinate system.

Since $\mathcal{F}^R$ is always changing with the positions of O_A and O_B, for derivation convenience, a local in orbit frame $\mathcal{F}^L$ is defined as such: origin is the origin $\mathcal{F}^R$, one axis is normal to the orbital plane, second one towards the velocity direction, third one complete the right hand coordinate system.

Figure 3-2 also shows the relationship between $\mathcal{F}^R$ and $\mathcal{F}^I$. Moving $\mathcal{F}^I$ to origin O_A is just for drawing convenience. Rotation matrix from $\mathcal{F}^R$ to $\mathcal{F}^I$ could be expressed as:

$$R_{R/I} = R(y,\, \theta_y)\, R(x,\, -\theta_x)\,, \tag{3–1}$$

where

$$\theta_x = \tan^{-1}\frac{d_x}{d_z}\,, \quad \theta_y = \sin^{-1}\frac{d_x}{d}\,. \tag{3–2}$$

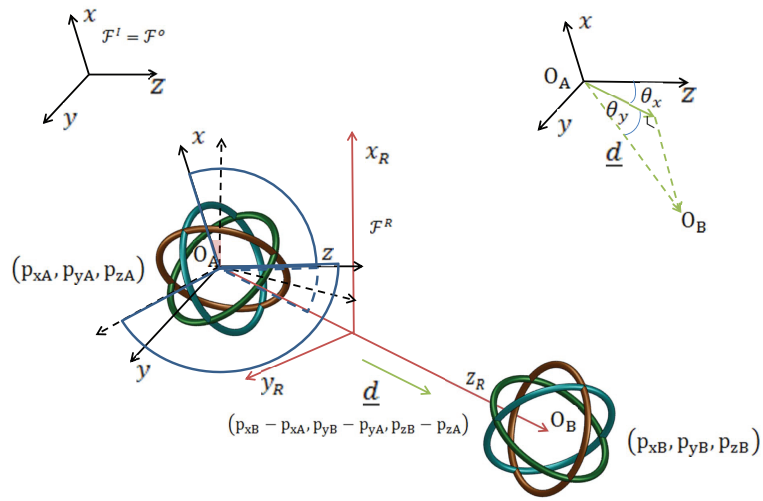

Figure 3-2. Definition of rotated reference coordinate system.

Also, d_x, d_y and d_z are three components of vector $\underline{d}$.

A very useful term, dominant axis, is defined to be the axis aligned with the approach axis for the docking mechanism. As shown in Figure 3-3, x_A and x_B are the dominant axes for satellite A and B respectively. The ring perpendicular to dominant axis is defined as the dominant ring. By defining a dominant axis, the control objective of achieving a relative attitude between satellites necessary for docking becomes determining how to align these dominant axes and twist about the co-axis after the alignment.

Now, starting with representation of orientations of A and B, a reduction the of degrees of freedom is discussed here. The 3-2-1 sequential Euler angle rotation is used for representing the orientations of body fixed coordinate system $\mathcal{F}^A$ and $\mathcal{F}^B$ with respect to $\mathcal{F}^R$.

Referring to Figure 3-3, rotation from $\mathcal{F}^R$ to $\mathcal{F}^B$ has been shown as: $\mathcal{F}^B$ is initially aligned with $\mathcal{F}^R$, then rotate δ about z_R, following by rotating and $\beta - \pi/2$ about body fixed axis y_B, then rotate ψ about body fixed axis x_B. Rotation matrix from $\mathcal{F}^R$ to $\mathcal{F}^B$ is expressed as:

$$R_{B/R} = R(x,\ \psi)\, R(y,\ \beta - \pi/2)\, R(z,\ \delta)\,. \tag{3–3}$$

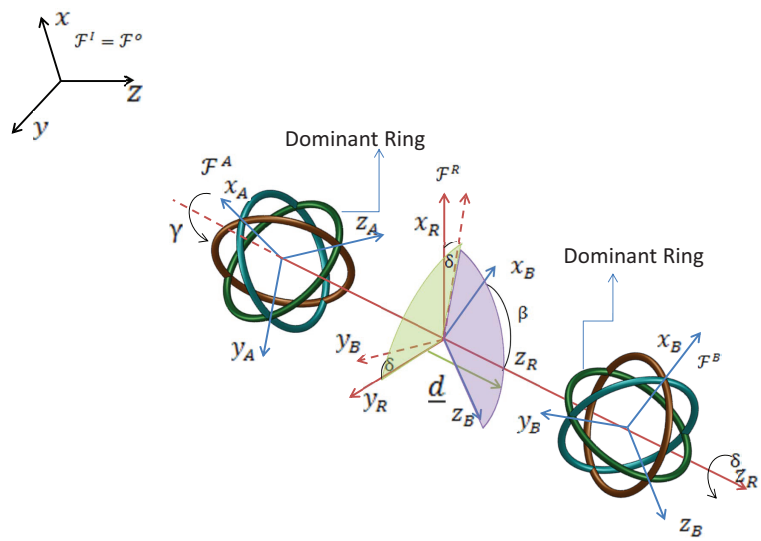

Figure 3-3. Relationship between body fixed frame and rotated reference frame.

It is similar to get $\mathcal{F}^A$: $\mathcal{F}^A$ is initially aligned with $\mathcal{F}^R$, then rotate γ about z_R, following by rotating and $\alpha - \pi/2$ about body fixed axis y_A, then rotate ϕ about body fixed axis x_A. Rotation matrix from $\mathcal{F}^R$ to $\mathcal{F}^A$ is expressed as:

$$R_{A/R} = R(x,\ \phi)\, R(y,\ \alpha - \pi/2)\, R(z,\ \gamma)\,. \tag{3–4}$$

Considering that we are dealing with alignment problem of two rings, recall some contents in Chapter 2. Per Section 2.3.4 and because of the axial symmetry of rings, rotations about x_A and x_B determining do not affect the force and torque generated by these two rings. Considering that the alignment problem is dealing with the relative attitude between two dominant rings, the 3-2 sequential Euler angle rotation could be used to identify the attitude of dominant rings. The third rotation about the dominant axis could be handled in the twist step.

Again, to emphasize the peculiarities of dynamics between current loops, we will start from deep space assumption. For deep space missions, orbital dynamics (the influence of earth gravity and geomagnetic field) is usually ignored. Deep space assumption is the base of derivations of this chapter's dynamic equations. Since in deep space assumption the orbit dynamics are not considered, the assumption that $\mathcal{F}^L$ is

aligned with $\mathcal{F}^I$ can be made. Chapter 5 will discuss more about the impact of ignoring the orbital dynamics and geomagnetic field on the performance of the controller.

3.2.2 Docking Strategy

As discussed in last section, the control objective of adjusting the relative attitude can be separated into two sequential steps: aligning the dominant axes with the distance vector (i.e., the z_R), followed by twisting the satellites about the aligned axis z_R to the final desired relative attitude.

Further, the alignment in 3-D reality can be obtained by breaking the procedure into two independent 2-D coplanar cases. First, align one dominant axis with z_R, then align another. Without losing generality, we choose to first align x_A with z_R. Details about how to decouple the 3-D case alignment case into 2-D coplanar cases are in Section 3.4, including the dynamics for each specific step.

Once the dominant axes are co-axial with z_R twisting the satellites about the co-axis is the last step for attitude adjustment. This step can be achieved but requires a reduction in the controlled degrees of freedom of the system as mentioned in last section.

Overall, Step 1 can be divided into 3 sequential steps: Step 1.A, Step 1.B, and Step 1.C. Once Step 1 is accomplished, Step 2 is just a 1-D distance control problem. See Figure 3-4.

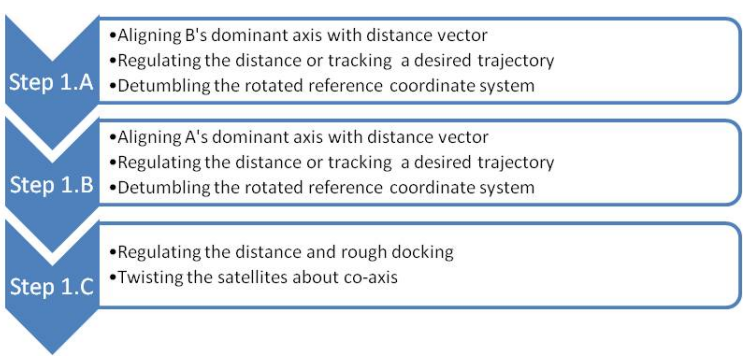

Figure 3-4. Subdivision for Step 1.

One important remark: in Step 1.A and Step 1.B, taking into account the problem of degree of freedom, torques act on Satellite A and Satellite B are set to be canceled by reaction wheels respectively.

3.3 Basic Dynamic Fundamental Equations

Momentum of rigid body A is denoted as $\underline{P}^A$. If we choose the center of mass c as reference point, $\underline{P}^A$ is given by:

$$\underline{P}_c^A = m\,\underline{v}_c\,, \tag{3–5}$$

in which, m is the mass of A, $\underline{v}_c$ is the velocity of c. For convenience of representation, $\underline{P}_c^A$ sometimes is simplified to be $\underline{P}^A$.

Angular momentum of rigid body A about reference point o is denoted as $\underline{H}_o^A$. If we choose the center of mass c as reference point, $\underline{H}_c^A$ is given by [7]

$$\underline{H}_c^A = I\,\underline{\omega}\,, \tag{3–6}$$

where $\underline{\omega}$ is angular velocity of A.

Generally, dynamic equations of rigid body A include translational equation and rotational equation.

$$\dot{\underline{P}}_c^A + [\underline{\omega}]^\times\,\underline{P}_c^A = \underline{f}_{ex}\,, \tag{3–7}$$

where $\underline{f}_{ex}$ is the external force act on body A.

$$\dot{\underline{H}}_c^A + [\underline{\omega}]^\times\,\underline{H}_c^A = \underline{\tau}_{ex}\,, \tag{3–8}$$

where $\underline{\tau}_{ex}$ is the external torque act on body A.

3.4 Dynamics for Specific Steps

3.4.1 Step 1.A

In this step, alignment of x_B with $\underline{d}$ (z_R) will be accomplished. Orientation of Satellite A is fixed. Comparing to the general coplanar case, in 3-D reality, alignment does not have to happen in plane $x_R z_R$. Therefore, an auxiliary coordinate system $\mathcal{F}^\delta$ is defined.

As shown in the Figure 3-5, $\mathcal{F}^{\delta}$ is initially aligned with $\mathcal{F}^{R}$, then rotates angle δ about axis z_R. The arrow of this rotation in the figure is just for showing the positive direction of δ. Rotation matrix from $\mathcal{F}^{R}$ to $\mathcal{F}^{\delta}$ is given by:

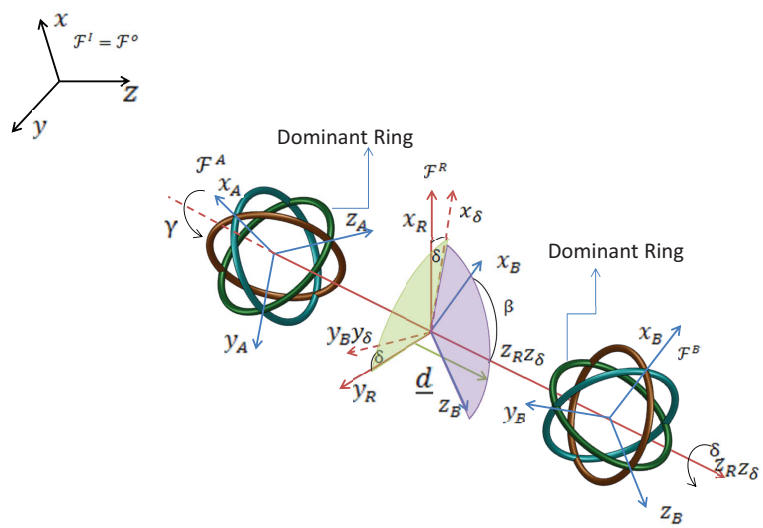

Figure 3-5. 3 dimensional (3-D) illustration for Step 1.A.

$$R_{\delta/R} = R(z,\ \delta) = \begin{bmatrix} \cos\delta & \sin\delta & 0 \\ -\sin\delta & \cos\delta & 0 \\ 0 & 0 & 1 \end{bmatrix}. \tag{3–9}$$

Now, it is easy to see that, dominant axis x_B and distance vector z_R both lie in plane $x_\delta z_\delta$. Therefore, Step 1.A is actually a simple coplanar case which occurs in this plane. In Figure 3-6, front view of plane $x_\delta z_\delta$ shows how this step reduces to the general 2-D coplanar case.

3.4.1.1 Translational dynamics

The dynamic equations for Step 1.A will be derived in coordinate system $\mathcal{F}^{\delta}$. Position vector of A and B in $\mathcal{F}^{\delta}$ can be expressed as:

$$^{\delta}\underline{p}_A = \begin{bmatrix} 0 & 0 & -\frac{d}{2} \end{bmatrix}^{\top}, \quad ^{\delta}\underline{p}_B = \begin{bmatrix} 0 & 0 & \frac{d}{2} \end{bmatrix}^{\top}. \tag{3–10}$$

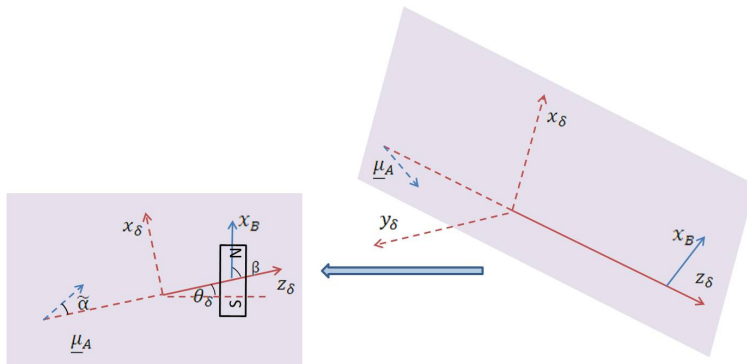

Figure 3-6. Front view of Step 1.A.

Choosing these A and B locations in $\mathcal{F}^\delta$ is for calculation convenience. Thus, momentums of A and B represented in $\mathcal{F}^\delta$ are given by

$$ {}^{\delta}\underline{P}^{A} = m_A \left({}^{\delta}\dot{\underline{p}}_A + {}^{\delta}\underline{\omega}_{\delta/I} \times {}^{\delta}\underline{p}_A \right), \quad {}^{\delta}\underline{P}^{B} = m_B \left({}^{\delta}\dot{\underline{p}}_A + {}^{\delta}\underline{\omega}_{\delta/I} \times {}^{\delta}\underline{p}_B \right), \tag{3–11} $$

in which, m_A and m_B are mass of A and B, ${}^{\delta}\underline{\omega}_{\delta/I}$ is the angular velocity of $\mathcal{F}^\delta$ with respect to inertial frame. Considering that in this 2-D coplanar case the motion happens occurs in plane, it does not change the rotation matrix from $\mathcal{F}^R$ to $\mathcal{F}^\delta$, $R_{\delta/R}$, which means angular velocity of $\mathcal{F}^\delta$ is the same of ${}^{\delta}\underline{\omega}_{\delta/I}$:

$$ {}^{\delta}\underline{\omega}_{\delta/I} = {}^{\delta}\underline{\omega}_{R/I} \,. \tag{3–12} $$

Due to the deep space assumption ($\mathcal{F}^I = \mathcal{F}^L$),

$$ {}^{\delta}\underline{\omega}_{\delta/I} = {}^{\delta}\underline{\omega}_{R/I} = {}^{\delta}\underline{\omega}_{R/L} = \begin{bmatrix} 0 \\ \dot{\theta}_\delta \\ 0 \end{bmatrix} . \tag{3–13} $$

Notice, in low earth orbit case, ${}^{\delta}\underline{\omega}_{L/I}$ is no longer zero. Chapter 5 shows more about this influence on the modeling and controller performance.

Substituting, we have:

$$ {}^{\delta}\underline{P}^{A} = m_A \begin{bmatrix} -\frac{d\,\dot{\theta}_\delta}{2} \\ 0 \\ -\frac{\dot{d}}{2} \end{bmatrix}, \quad {}^{\delta}\underline{P}^{B} = m_B \begin{bmatrix} \frac{d\,\dot{\theta}_\delta}{2} \\ 0 \\ \frac{\dot{d}}{2} \end{bmatrix}. \tag{3–14} $$

Recall (3–7), we have:

$$ {}^{\delta}\dot{\underline{P}}^{A} + {}^{\delta}\underline{\omega}_{\delta/I} \times {}^{\delta}\underline{P}^{A} = {}^{\delta}\underline{F}^{A}. \tag{3–15} $$

Substitute (3–14) to (3–15), we got:

$$ m_A \begin{bmatrix} -\frac{d\,\ddot{\theta}_\delta}{2} - \frac{\dot{d}\,\dot{\theta}_\delta}{2} - \frac{\dot{d}\,\dot{\theta}_\delta}{2} \\ 0 - \frac{\ddot{d}}{2} + \frac{d\,\dot{\theta}_\delta^2}{2} \end{bmatrix} = {}^{\delta}\underline{F}_A. \tag{3–16} $$

In $\mathcal{F}^{\delta}$, ${}^{\delta}\underline{\mu}_A$ only gives components in plane $x_\delta z_\delta$,

$$ {}^{\delta}\underline{\mu}_A = \begin{bmatrix} \mu_{x\delta} \\ 0 \\ \mu_{z\delta} \end{bmatrix} = \mu_A \begin{bmatrix} \sin\tilde{\alpha} \\ 0 \\ \cos\tilde{\alpha} \end{bmatrix}. \tag{3–17} $$

Also, $\underline{\mu}_B$ in this step is only given by dominant ring of B:

$$ \underline{\mu}_B = \mu_{Bx}\,\underline{\hat{X}}_B. \tag{3–18} $$

Substitute ${}^{\delta}\underline{\mu}_A$ into to (2–47), force act on A is given by:

$$ {}^{\delta}\underline{F}_A = \frac{3\,\mu_0}{4\,\pi}\,\frac{\mu_{Bx}}{d^4} \begin{bmatrix} -\mu_{z\delta}\sin\beta - \mu_{x\delta}\cos\beta \\ 0 \\ 2\,\mu_{z\delta}\cos\beta - \mu_{x\delta}\sin\beta \end{bmatrix}. \tag{3–19} $$

Then, assume $m_A = m_B = 3\,m$, where m is the mass of each coil, after some reorganization, translational dynamics equations are given by:

$$\ddot{\theta}_\delta = \frac{1}{m}\,\frac{\mu_0}{2\,\pi}\,\frac{\mu_{Bx}}{d^5}\,(\mu_{z\delta}\sin\beta + \mu_{x\delta}\cos\beta) - \frac{2\,\dot{d}\,\dot{\theta}_\delta}{d}\,, \tag{3–20}$$

$$\ddot{d} = -\frac{1}{m}\,\frac{\mu_0}{2\,\pi}\,\frac{\mu_{Bx}}{d^4}\,(2\mu_{z\delta}\cos\beta - \mu_{x\delta}\sin\beta) + d\,\dot{\theta}_\delta^2\,. \tag{3–21}$$

Since for the system of satellite A and B, there is no external force, the change in momentum of this whole system equals zero. Thus taking the time derivative of ${}^{\delta}\underline{P}_B$ will give out the exact two equations.

3.4.1.2 Rotational dynamics

Since in Step 1.A, attitude of satellite A is fixed, rotational dynamic equation for B will be derived. Angular momentum of B about center of mass represented in $\mathcal{F}^\delta$ is as follows:

$${}^{\delta}\underline{H}_c^B = {}^{\delta}I_B\,{}^{\delta}\underline{\omega}_{B/I}\,, \tag{3–22}$$

in which ${}^{\delta}I_B$ is the inertia matrix of B about center of mass represented in $\mathcal{F}^\delta$. By using transformation of inertia matrix, we have:

$${}^{\delta}I_B = R_{B/\delta}^{\top}\,{}^{B}I_B\,R_{B/\delta}\,, \tag{3–23}$$

where $R_{B/\delta}$ is rotation matrix from $\mathcal{F}^\delta$ to body fixed frame:

$$R_{B/\delta} = R(y,\,\beta - \frac{\pi}{2})\,. \tag{3–24}$$

As well, for three rings with radius r, mass m,

$${}^{B}I_B = 2\,m\,r^2\begin{bmatrix}1 & 0 & 0\\ 0 & 1 & 0\\ 0 & 0 & 1\end{bmatrix}. \tag{3–25}$$

Since $R_{B/\delta}^{\top} R_{B/\delta} = I_{identity}$,

$$
{}^{\delta}I_B = 2\,m\,r^2 \begin{bmatrix} 1 & 0 & 0 \\ 0 & 1 & 0 \\ 0 & 0 & 1 \end{bmatrix} . \tag{3–26}
$$

Note, in this thesis, only the mass and inertia of the three coils is used in the analysis. However, in future simulations, these terms can easily be updated to include the full satellite mass and inertia.

Angular velocity of B with respect to inertia frame represented in $\mathcal{F}^{\delta}$, ${}^{\delta}\underline{\omega}_{B/I}$ is given by:

$$
{}^{\delta}\underline{\omega}_{B/I} = {}^{\delta}\underline{\omega}_{B/\delta} + {}^{\delta}\underline{\omega}_{\delta/I} , \tag{3–27}
$$

where

$$
{}^{\delta}\underline{\omega}_{B/\delta} = \begin{bmatrix} 0 \\ \dot{\beta} \\ 0 \end{bmatrix} , \quad {}^{\delta}\underline{\omega}_{\delta/I} = \begin{bmatrix} 0 \\ \dot{\theta}_{\delta} \\ 0 \end{bmatrix} . \tag{3–28}
$$

Substituting, we have

$$
{}^{\delta}\underline{H}_c^B = {}^{\delta}I_B\,{}^{\delta}\underline{\omega}_{B/I} = 2\,m_B\,r_B^2 \begin{bmatrix} 0 \\ \dot{\beta} + \dot{\theta}_{\delta} \\ 0 \end{bmatrix} \tag{3–29}
$$

Take time derivative of ${}^{\delta}\underline{H}_c^B$,

$$
{}^{\delta}\dot{\underline{H}}_c^B + [\underline{\omega}_{\delta/I}]^{\times}\,{}^{\delta}\underline{H}_c^B = {}^{\delta}\underline{\tau}_B . \tag{3–30}
$$

Substitute (3–28) and (3–29) into (3–30), we have rotational dynamics equations:

$$
2\,m\,r^2 \begin{bmatrix} 0 \\ \ddot{\beta} + \ddot{\theta}_{\delta} \\ 0 \end{bmatrix} = {}^{\delta}\underline{\tau}_B . \tag{3–31}
$$

Recall (2–50), we have:

$$^{\delta}\underline{\tau}_B = -\frac{\mu_0}{4\,\pi}\,\frac{\mu_B}{d^3}\,(2\,\mu_{z\delta}\sin\beta + \mu_{x\delta}\cos\beta)\,. \tag{3–32}$$

Combine (3–31) and (3–32), we have:

$$\ddot{\beta} = -\frac{\mu_0}{8\,\pi}\,\frac{\mu_B}{d^3\,m\,r^2}\,(2\,\mu_{z\delta}\sin\beta + \mu_{x\delta}\cos\beta) - \ddot{\theta}_\delta\,. \tag{3–33}$$

Then, we have:

$$\ddot{\beta} = -\frac{\mu_0}{8\,\pi}\,\frac{\mu_B}{d^3\,m\,r^2}\,(2\,\mu_{z\delta}\sin\beta+\mu_{x\delta}\cos\beta)-\frac{1}{m}\,\frac{\mu_0}{2\,\pi}\,\frac{\mu_{Bx}}{d^5}\,(\mu_{z\delta}\sin\beta+\mu_{x\delta}\cos\beta)+\frac{2\,\dot{d}\,\dot{\theta}_\delta}{d}\,. \tag{3–34}$$

Remember the $\underline{\mu}_A$ is generated by three orthogonal rings, representation in $\mathcal{F}^\delta$. Therefore, $^{\delta}\underline{\mu}_A$ must be transferred back to $\mathcal{F}^A$. If we cancel the torque acting on satellite A by momentum management, rotation matrix from $\mathcal{F}^R$ to $\mathcal{F}^R$, $R_{A/R}$, will be a constant matrix. Also, satellite B only rotates in the plane $x_\delta z_\delta$. Hence,

$$^{A}\underline{\mu}_A = R_{A/R}^{\top}\,{}^{R}\underline{\mu}_A = R_{A/R}^{\top}\,R_{\delta/R}^{\top}\,{}^{\delta}\underline{\mu}_A\,. \tag{3–35}$$

3.4.2 Step 1.B

Step 1.B happens in plane $x_\gamma z_\gamma$, in which x_A and z_R lie. Dynamics equations for this step is derived in coordinate system $\mathcal{F}^\gamma$. An auxiliary coordinate system $\mathcal{F}^\gamma$ is defined as follows. As shown in the Figure 3-7 and 3-8, $\mathcal{F}^\gamma$ is initially aligned with $\mathcal{F}^R$, then rotates angle γ about axis z_R. The arrow of this rotation in the figure is just for showing the positive direction of γ. Rotation matrix from $\mathcal{F}^R$ to $\mathcal{F}^\gamma$ is given by:

$$R_{\gamma/R} = R(z,\,\gamma)\,. \tag{3–36}$$

Derivation of dynamic equations is similar to Step 1.A. Remember, orientation of satellite B is set to be fixed in this step.

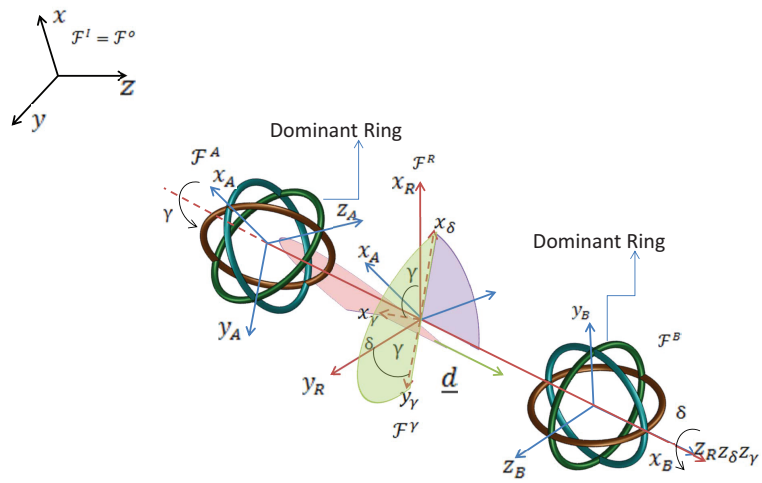

Figure 3-7. 3-D illustration for Step 1.B.

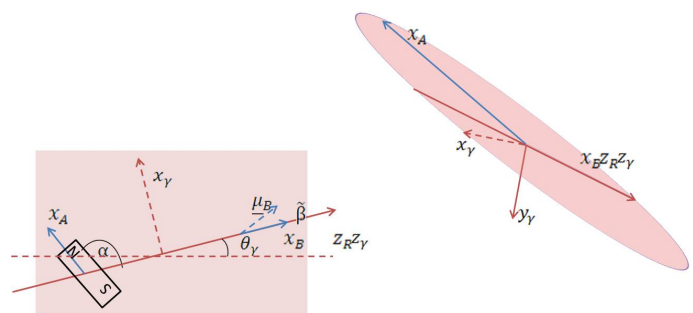

Figure 3-8. Front view of Step 1.B.

3.4.2.1 Translational dynamics

Basically, there is no difference from Step 1.A's dynamics modeling except for deriving in coordinate system $\mathcal{F}^R$. To save space, only important results will be shown in this section.

Translational dynamics equation is given by:

$$3\,m \begin{bmatrix} -\frac{d\,\ddot{\theta}_\gamma}{2} - \frac{\dot{d}\,\dot{\theta}_\gamma}{2} - \frac{\dot{d}\,\dot{\theta}_\gamma}{2} \\ 0 \\ -\frac{\ddot{d}}{2} + \frac{d\,\dot{\theta}_\gamma^2}{2} \end{bmatrix} = {}^{\gamma}\underline{F}_A\,. \tag{3–37}$$

In $\mathcal{F}^{\gamma}$, ${}^{\gamma}\underline{\mu}_B$ only gives components in plane $x_\gamma z_\gamma$,

$$ {}^{\gamma}\underline{\mu}_B = \begin{bmatrix} \mu_{x\gamma} \\ 0 \\ \mu_{z\gamma} \end{bmatrix} = \mu_B \begin{bmatrix} \sin\tilde{\beta} \\ 0 \\ \cos\tilde{\beta} \end{bmatrix} \tag{3–38} $$

Also, $\underline{\mu}_A$ in this step is only given by dominant ring of A:

$$ \underline{\mu}_A = \mu_{Ax}\,\underline{\hat{x}}_A\,. \tag{3–39} $$

Substitute ${}^{\delta}\underline{\mu}_B$ into to (2–47), force acting on A is given by:

$$ {}^{\gamma}\underline{F}_A = \frac{3\,\mu_0}{4\,\pi}\,\frac{\mu_{Ax}}{d^4} \begin{bmatrix} -\mu_{x\gamma}\cos\alpha - \mu_{z\gamma}\sin\alpha \\ 0 \\ 2\,\mu_{z\gamma}\cos\alpha - \mu x\gamma\sin\alpha \end{bmatrix}. \tag{3–40} $$

Reorganizing,

$$ \ddot{\theta}_\gamma = \frac{1}{m}\,\frac{\mu_0}{2\,\pi}\,\frac{\mu_{Ax}}{d^5}\,(\mu_{x\gamma}\cos\alpha + \mu_{z\gamma}\sin\alpha) - \frac{2\,\dot{d}\,\dot{\theta}_\gamma}{d}\,, \tag{3–41} $$

$$ \ddot{d} = \frac{1}{m}\,\frac{\mu_0}{2\,\pi}\,\frac{\mu_{Ax}}{d^4}\,(2\,\mu_{z\gamma}\cos\alpha - \mu_{x\gamma}\sin\alpha) + d\,\dot{\theta}_\gamma^2\,. \tag{3–42} $$

3.4.2.2 Rotational dynamics

Similarly, only main equations will be shown for Step 1.B.

$$ 2\,m\,r^2 \begin{bmatrix} 0 \\ \ddot{\alpha} + \ddot{\theta}_\gamma \\ 0 \end{bmatrix} = {}^{\gamma}\underline{\mathcal{T}}_A\,. \tag{3–43} $$

By using (2–49), torque act on A is given by:

$$ {}^{\gamma}\underline{\mathcal{T}}_A = \begin{bmatrix} 0 \\ -\frac{\mu_0}{8\,\pi}\,\frac{\mu_A\,\mu_B}{d^3}\,(2\,\mu_{z\gamma}\sin\alpha + \mu_{x\gamma}\cos\alpha) \\ 0 \end{bmatrix} \tag{3–44} $$

Therefore

$$\ddot{\alpha} = -\frac{\mu_0}{8\,\pi}\,\frac{\mu_{Ax}}{d^3\,m\,r^2}\,(2\,\mu_{z\gamma}\sin\alpha + \mu_{x\gamma}\cos\alpha) - \frac{1}{m}\,\frac{\mu_0}{2\,\pi}\,\frac{\mu_B}{d^5}\,(\mu_{x\gamma}\cos\alpha + \mu_{z\gamma}\sin\alpha) + \frac{2\,\dot{d}\,\dot{\theta}_\gamma}{d}\,. \tag{3–45}$$

Transfer ${}^{\gamma}\underline{\mu}_B$ to $\mathcal{F}^B$:

$${}^{B}\underline{\mu}_B = R^{\top}_{B/R}\,R^{\top}_{\gamma/R}\,{}^{\gamma}\underline{\mu}_B\,. \tag{3–46}$$

3.4.3 Step 1.C

After Step 1.A and Step 1.B, both two dominant axes are aligned with distance vector. Controlling the distance between of A and B now reduces to a 1-D attraction or repulsive case. When twisting other coils which are perpendicular to the dominant rings about co-axial, we have 2 sate variables d and angle difference $(\varphi - \psi)$ with only one input $(\mu_{Ay}\ \mu_{By})$ which means that distance control cannot be guaranteed. However, by introducing a 'rough docking' approach which is defined as distance maintenance by using mechanical contacts, the twisting the satellite about co-axis could be accomplished. In this step,

$${}^{A}\underline{\mu}_A = \begin{bmatrix} 0 \\ \mu_{Ay} \\ 0 \end{bmatrix}, \quad {}^{B}\underline{\mu}_B = \begin{bmatrix} 0 \\ \mu_{By} \\ 0 \end{bmatrix}. \tag{3–47}$$

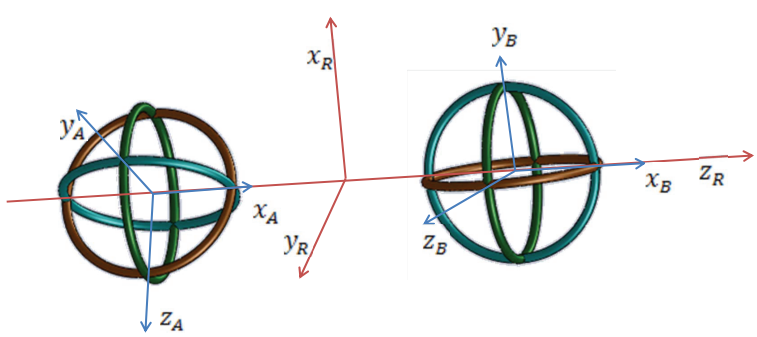

Figure 3-9. 3-D illustration for Step 1.C.

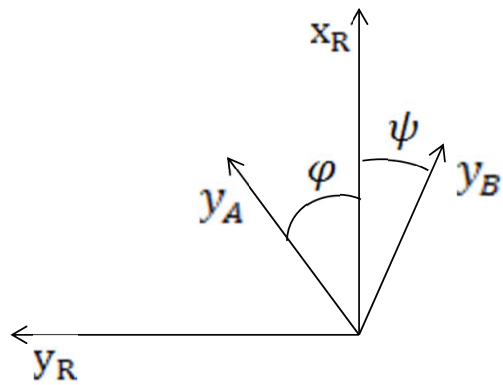

Figure 3-10. Front view of Step 1.C.

3.4.3.1 Translational dynamics

From Section 2.3.3, we have the force generated by the μ_{Ay} and μ_{By} components:

$$\underline{F}_A = \frac{3\,\mu_0\,\mu_{Ay}\,\mu_{By}}{4\,\pi\,d^4}\cos(\varphi-\psi)\,\hat{\underline{z}}_R\,, \quad \underline{F}_B = \frac{3\,\mu_0\,\mu_{Ay}\,\mu_{By}}{4\,\pi\,d^4}\cos(\varphi-\psi)\,\hat{\underline{z}}_R\,. \tag{3–48}$$

Sum up,

$$\underline{F}_A = \frac{3\,\mu_0\,\mu_{Ay}\,\mu_{By}}{4\,\pi\,d^4}\cos(\varphi-\psi)\,\hat{\underline{z}}_R\,, \quad \underline{F}_B = \frac{3\,\mu_0\,\mu_{Ay}\,\mu_{By}}{4\,\pi\,d^4}\cos(\varphi-\psi)\,\hat{\underline{z}}_R\,. \tag{3–49}$$

For translational dynamics there is only one state variable, d. Time derivative of momentum for A could be expressed:

$$-\,3\,m\,\frac{\ddot{d}}{2} = \underline{F}_A\,. \tag{3–50}$$

Reorganizing:

$$\ddot{d} = \frac{\mu_0\,\mu_{Ay}\,\mu_{By}}{2\,m\,\pi\,d^4}\cos(\varphi-\psi)\,. \tag{3–51}$$

3.4.3.2 Rotational dynamics

From Section 2.3.3, we have the torque generated by the μ_{Ay} and μ_{By}:

$$\underline{\tau}_A = -\frac{\mu_0\,\mu_{Ay}\,\mu_{By}}{4\,\pi\,d^3}\sin(\varphi-\psi)\,\hat{\underline{z}}_R\,, \quad \underline{\tau}_B = \frac{\mu_0\,\mu_{Ay}\,\mu_{By}}{4\,\pi\,d^3}\sin(\varphi-\psi)\,\hat{\underline{z}}_R\,. \tag{3–52}$$

Time derivative of angular momentums for A and B are derived as:

$$\begin{bmatrix} 0 \\ 0 \\ 2\,m\,r^2\,\ddot{\varphi} \end{bmatrix} = \underline{\tau}_A\,, \quad \begin{bmatrix} 0 \\ 0 \\ 2\,m\,r^2\,\ddot{\psi} \end{bmatrix} = \underline{\tau}_B\,. \tag{3–53}$$

Subtracting:

$$\ddot{\varphi} - \ddot{\psi} = -\frac{\mu_0\,\mu_{Ay}\,\mu_{By}}{4\,\pi\,m\,r^2}\,\sin(\varphi - \psi)\,. \tag{3–54}$$

3.4.4 Step 2

In Step 2, the relative attitude has been adjusted by Step 1. Hence, only thing needing to be accomplished in this step is generating attraction or repulsive force repulsive with docking mechanism. Since the force direction is along the distance vector, it is basically a 1-D case. In this step, the dominant rings are used to generate the force.

$$^{A}\underline{\mu}_A = \begin{bmatrix} \mu_{Ax} \\ 0 \\ 0 \end{bmatrix}, \quad ^{B}\underline{\mu}_B = \begin{bmatrix} \mu_{Bx} \\ 0 \\ 0 \end{bmatrix}. \tag{3–55}$$

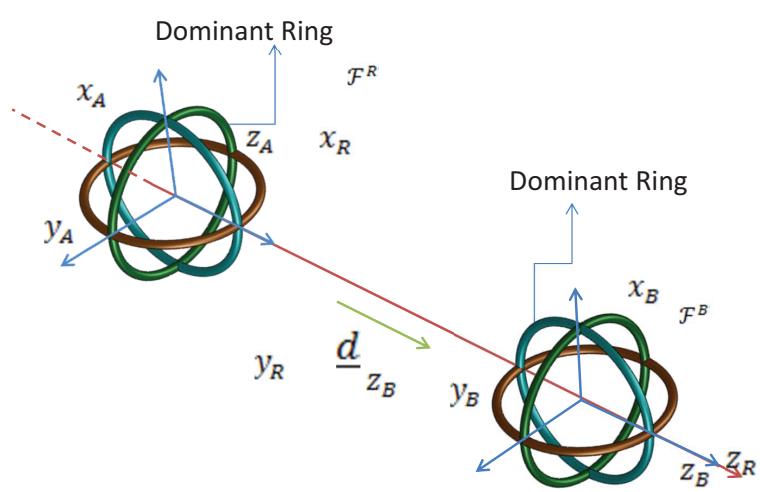

Figure 3-11. 3-D illustration for Step 2.

From Section 2.3.2, the force and torque for 1-D case has been derived:

$$\underline{F}_A = \frac{3\,\mu_0}{2\,\pi}\,\frac{\mu_{Ax}\,\mu_{Bx}}{d^4}\,\hat{\underline{z}}_R\,, \quad \underline{F}_B = -\frac{3\,\mu_0}{2\,\pi}\,\frac{\mu_{Ax}\,\mu_{Bx}}{d^4}\,\hat{\underline{z}}_R\,, \tag{3–56}$$

Time derivative of momentum for A is derived as:

$$-\,3\,m\,\frac{\ddot{d}}{2} = \underline{F}_A\,. \tag{3–57}$$

Reorganizing:

$$\ddot{d} = -\frac{\mu_0}{\pi\,m}\,\frac{\mu_{Ax}\,\mu_{Bx}}{d^4}\,. \tag{3–58}$$

Per the above, the set of dynamic models that capture the behavior of the two satellites in the presented docking strategy will now be used for deriving the controller for the magnetic coil docking system. Design details and simulated results are presented in the next chapter.

CHAPTER 4
CONTROL LAWS AND SIMULATION RESULTS

4.1 Overview

In this chapter, the overall control strategy for the magnetic coil docking approach is shown. Details of the controller design for each step in the docking is presented. This is followed by simulation results of the individual controllers and demonstration of the sequential combination of these controllers. All the simulations are performed using Matlab and Simulink.

Important assumptions are:

- Full relative position and attitude estimation can be achieved, including relationship between $\mathcal{F}^R$ and body fixed frames $\mathcal{F}^A$ and $\mathcal{F}^B$. Which means that both $R_{B/R}$ and $R_{A/R}$ are reachable.
- The 3-2-1 sequential Euler angles (α, β, γ, δ, φ and ψ) can be determined from rotation matrix.
- For convenience, the d, α, β, γ, δ, φ and ψ are the state variables directly used in simulation.
- The relative position can be used to determine θ_δ and θ_γ.
- First order time derivative of d, α, β, γ, δ, φ, ψ, θ_δ and θ_γ can be measured. Determining $\dot{\alpha}$, $\dot{\beta}$, $\dot{\gamma}$, $\dot{\delta}$, $\dot{\varphi}$, and $\dot{\psi}$ is reasonable if the angular velocity sensors is equipped. Relative velocity estimation between two satellites will give $\dot{d}$, $\dot{\theta}_\delta$, and $\dot{\theta}_\gamma$.

Since, position and attitude estimation is a whole new area, this thesis will focus on the dynamics and controller design for each step in the docking strategy where all the states and their time derivatives are measured directly and/or estimated.

4.2 Control Strategy

Per the control strategy mentioned in Section 3.2.2, the corresponding control flow chart is designed to more fully demonstrate the approach of this thesis refer to Figure 4-3 and 4-4. To help visualizing each step of this flow chart, Figure 1-3 is repeated here.

Note: in this thesis, detumbling $\mathcal{F}^R$ or θ_δ and θ_γ is defined as such, considering these two satellites as a system, preventing the rotation of two satellites about the center of mass of this system. Note, it is different from detumbling a satellite which means stabilizing the attitude of this satellite.

Also, a 'rough docking' approach is defined as distance maintenance by using mechanical contacts. Figure 4-2 has shown a suitable docking mechanism. This foldable docking mechanism [20] gives the distance constraint as well as the circumferential constraint, meanwhile, it leaves one degree of freedom for twisting about the co-axial.

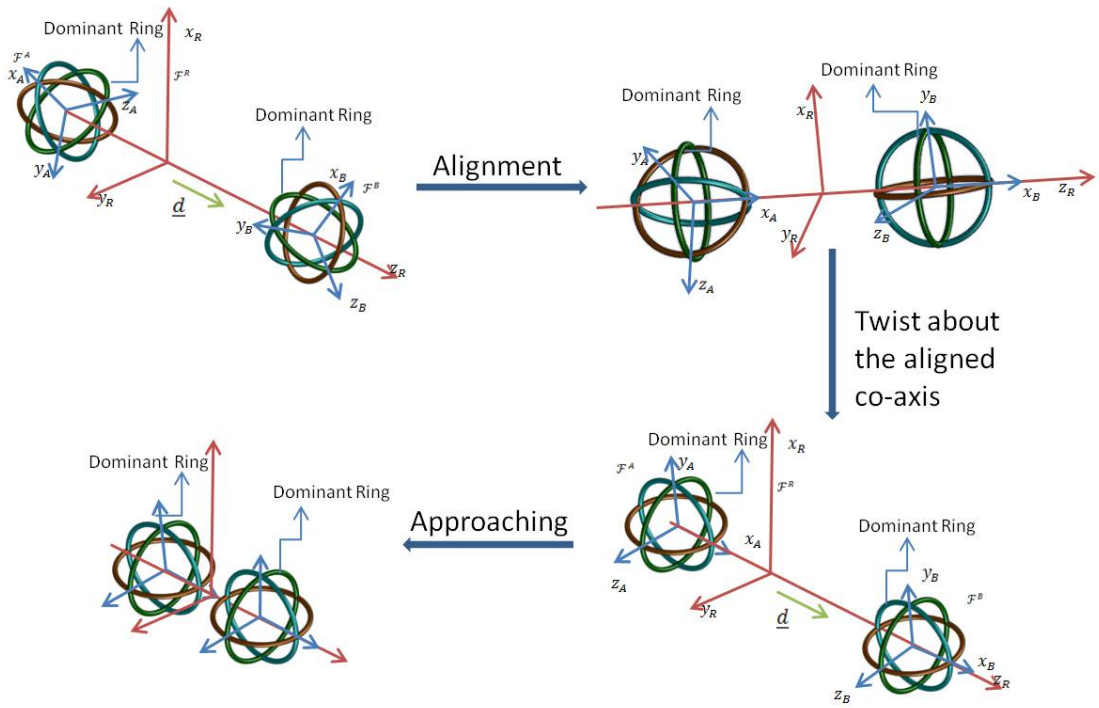

Figure 4-1. Repeat electromagnetic docking strategy.

Figure 4-5 shows the corresponding control diagram and its implementation as used in simulation. The control strategy is implemented to this two satellite system by using a multi-port trigger and switch. To guarantee the input is implementable, input saturation is necessary. Disturbance D and D_N are introduced to examine the robustness of the controllers.

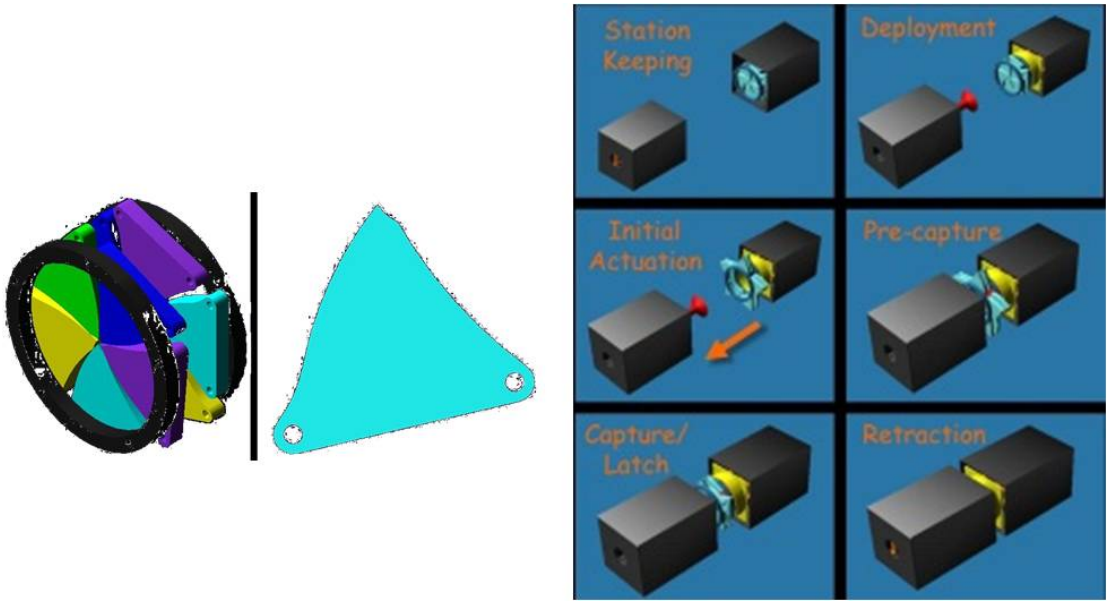

Figure 4-2. Rough docking mechanism: foldable docking Mechanism

As indicated in prior chapters, the control is achieved by a combination of controllers where each controller is designed using the corresponding dynamic model for the specific step in the alignment and docking process. As shown in the flow chart and control diagram, there are steps 1.A., 1.B. and 2 with transitional modes (e.g., steps 1.A.0, 1.A.1/1.B.0, 1.B.1) between controllers involving the reaction wheel states. The transitional modes use each satellite's reaction wheels to constrain the satellite behavior such that its dynamics can be approximated as the 2-D cases presented in Chapter 3. Thus, several control trigger indices are defined for judging steps completed or not, switching from one step's controller to the next controller. Criterions of these triggers will be defined later in the simulation section.

4.3 Controller Design for Each Step

Referring to [10], Lyapunov based high gain robust controller design methodology is applied in following controller designs.

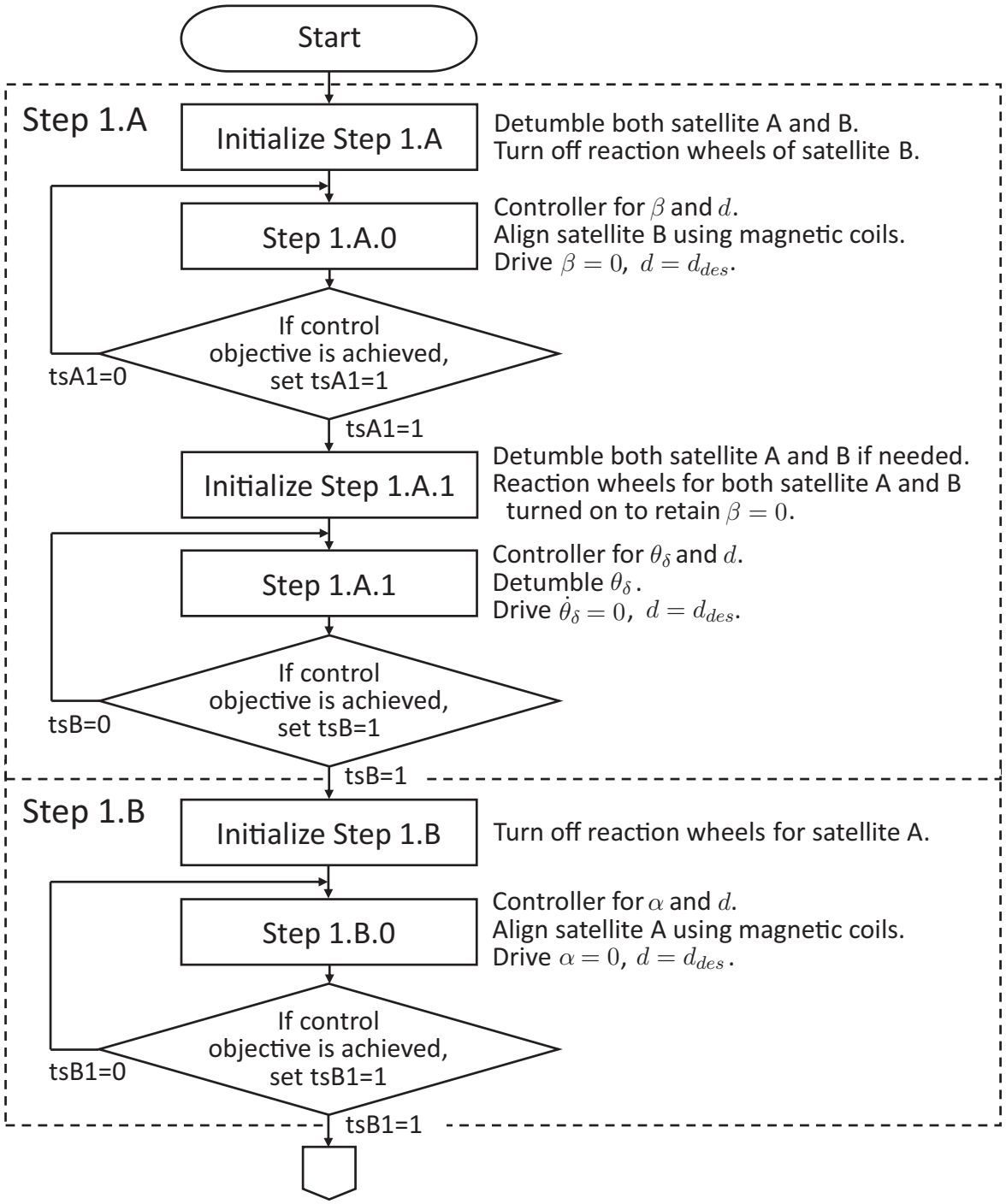

Figure 4-3. Control flow chart part 1.

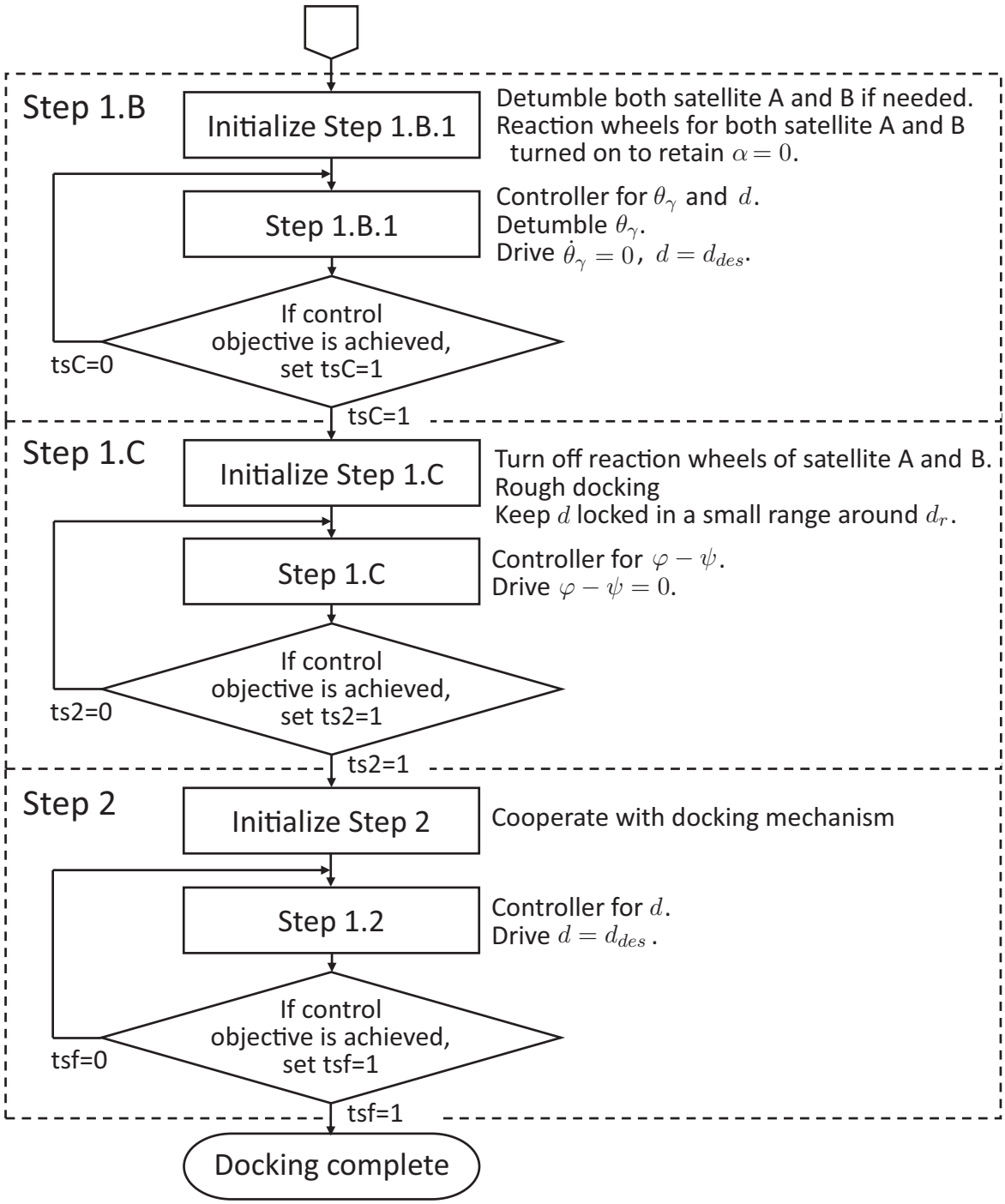

Figure 4-4. Control flow chart part 2.

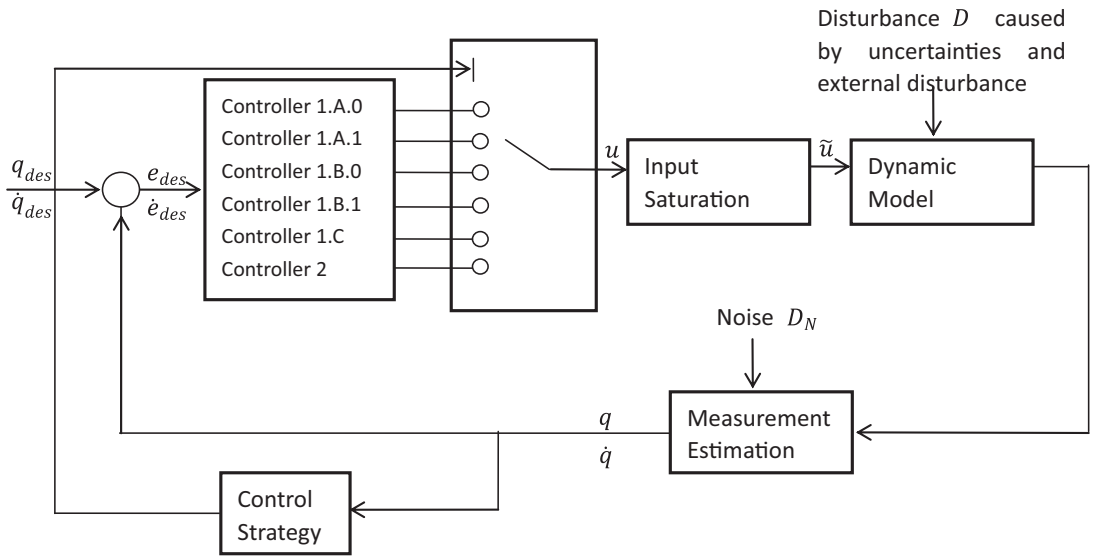

Figure 4-5. Control diagram.

4.3.1 Controller for Step 1.A

Recall the dynamics equations for Step 1.A:

$$\ddot{\theta}_\delta = \frac{1}{m}\frac{\mu_0}{2\,\pi}\frac{\mu_B}{d^5}\left(\mu_{z\delta}\sin\beta + \mu_{x\delta}\cos\beta\right) - \frac{2\,\dot{d}\,\dot{\theta}_\delta}{d}\,, \tag{4–1}$$

$$\ddot{d} = -\frac{1}{m}\frac{\mu_0}{2\,\pi}\frac{\mu_B}{d^4}\left(2\,\mu_{z\delta}\cos\beta - \mu_{x\delta}\sin\beta\right) + d\,\dot{\theta}_\delta^2\,, \tag{4–2}$$

$$\ddot{\beta} = -\frac{\mu_0}{8\,\pi}\frac{\mu_B}{d^3\,m\,r^2}\left(2\,\mu_{z\delta}\sin\beta + \mu_{x\delta}\cos\beta\right) - \frac{1}{m}\frac{\mu_0}{2\,\pi}\frac{\mu_B}{d^5}\left(\mu_{z\delta}\sin\beta + \mu_{x\delta}\cos\beta\right) + \frac{2\,\dot{d}\,\dot{\theta}_\delta}{d}\,. \tag{4–3}$$

Notice that there are 3 states variables in this system, yet only two inputs $\mu_{x\delta}\,\mu_B$ and $\mu_{z\delta}\,\mu_B$ could be supplied. Comparing to the control objective in this step (shown in Figure 3-4), controlling β is for the purpose of aligning B's dominant axis with distance vector, controlling d gives the ability of regulating the distance or tracking a desired trajectory, controlling θ_δ is for detumbling the rotated reference coordinate system $\mathcal{F}^R$.

To avoid collision, controlling d should always take precedence over other two objectives. Thus, we divided this step into two small steps: control d and β to achieve the control objective of aligning, set attitude of satellite B to be fixed and drive θ_δ to be zero. Between these two small steps, a trigger switch should be designed.

4.3.1.1 Step 1.A.0 control of d and β

To keep the controller design process concise, replace $\mu_{z\delta}\,\mu_{Bx}$ and $\mu_{x\delta}\,\mu_{Bx}$ with u_1 and u_2,

$$\begin{bmatrix} \ddot{d} \\ \ddot{\beta} \end{bmatrix} = \begin{bmatrix} -\frac{1}{m}\,\frac{\mu_0}{\pi}\,\frac{1}{d^4}\cos\beta & \frac{1}{m}\,\frac{\mu_0}{\pi}\,\frac{1}{d^4}\sin\beta \\ -\left(\frac{\mu_0}{4\,\pi}\,\frac{1}{d^3\,m\,r^2} + \frac{1}{m}\,\frac{\mu_0}{2\,\pi}\,\frac{1}{d^5}\right)\sin\beta & -\left(\frac{\mu_0}{8\,\pi}\,\frac{1}{d^3\,m\,r^2} + \frac{1}{m}\,\frac{\mu_0}{2\,\pi}\,\frac{1}{d^5}\right)\cos\beta \end{bmatrix} \begin{bmatrix} u_1 \\ u_2 \end{bmatrix} + \begin{bmatrix} 2\,d\,\dot{\theta}_\delta^2 \\ \frac{d\,\dot{\theta}_\delta^2}{d} \end{bmatrix}, \tag{4–4}$$

and reorganize dynamics model as such a form:

$$\underline{\ddot{q}} = B(\underline{q},\,\underline{\dot{q}})\,\underline{u} + G(\underline{q},\,\underline{\dot{q}}) + D\,, \tag{4–5}$$

in which

$$\begin{aligned} \underline{q} &= \begin{bmatrix} d \\ \beta \end{bmatrix}, \quad \underline{\dot{q}} = \begin{bmatrix} \dot{d} \\ \dot{\beta} \end{bmatrix}, \quad \underline{\ddot{q}} = \begin{bmatrix} \ddot{d} \\ \ddot{\beta} \end{bmatrix}, \quad \underline{u} = \begin{bmatrix} u_1 \\ u_2 \end{bmatrix}, \\ B &= \begin{bmatrix} -\frac{1}{m}\,\frac{\mu_0}{\pi}\,\frac{1}{d^4}\cos\beta & \frac{1}{m}\,\frac{\mu_0}{\pi}\,\frac{1}{d^4}\sin\beta \\ -\left(\frac{\mu_0}{4\,\pi}\,\frac{1}{d^3\,m\,r^2} + \frac{1}{m}\,\frac{\mu_0}{2\,\pi}\,\frac{1}{d^5}\right)\sin\beta & -\left(\frac{\mu_0}{8\,\pi}\,\frac{1}{d^3\,m\,r^2} + \frac{1}{m}\,\frac{\mu_0}{2\,\pi}\,\frac{1}{d^5}\right)\cos\beta \end{bmatrix}, \\ G &= \begin{bmatrix} 2\,d\,\dot{\theta}_\delta^2 \\ \frac{d\,\dot{\theta}_\delta^2}{d} \end{bmatrix}, \end{aligned} \tag{4–6}$$

and $\underline{D} \in \mathbb{R}^2$ is unknown disturbance caused by the model inaccuracy or some other factors.

Control objective are set to be:

$$\underline{e} = \underline{q} - \underline{q}_{des} \to \underline{0}\,, \quad \underline{\dot{e}} = \underline{\dot{q}} - \underline{\dot{q}}_{des} \to \underline{0}\,, \tag{4–7}$$

in which $\underline{q}_{des}$ is the desire trajectory for $\underline{q}$, $\underline{\dot{q}}_{des}$ is time derivative of $\underline{\dot{q}}$.

Before design of the controller, some properties should be proved or assumed as follows [a new class of modular adaptive controllers, [12]. The B^{-1} is assumed to exist. The $\underline{q}_{des}$ is designed such that n-th order of time derivative of $\underline{q}_{des}$ exists and is

bounded. If $\underline{q},\ \underline{\dot{q}} \in \mathcal{L}_\infty$, then $B,\ G,\ D \in \mathcal{L}_\infty$ ($\mathcal{L}_\infty$ means being bounded). For matrix B, $\underline{q},\ \underline{\dot{q}} \in \mathcal{L}_\infty \Rightarrow B_{ij} \in \mathcal{L}_\infty$ (refer to Appendix A), and $B_{ij} \in \mathcal{L}_\infty \Rightarrow B$. Also, for vector G, $\underline{q},\ \underline{\dot{q}} \in \mathcal{L}_\infty \Rightarrow G_i \in \mathcal{L}_\infty$, then $|G| = \sqrt{G_1^2 + G_2^2}$ is bounded too. The boundedness about unknown disturbance D must be assumed.

To prove B^{-1} exists, from the far-field model assumption in Section 2.3.1 we have $r \ll d$. Thus r^2/d^2, a higher order term for r/d, $r^2/d^2 = 0$ can be assumed. Then, in matrix B, the following approximation could be made:

$$\left(\frac{\mu_0}{4\,\pi}\,\frac{1}{d^3\,m\,r^2} + \frac{1}{m}\,\frac{\mu_0}{2\,\pi}\,\frac{1}{d^5}\right)\sin\beta = \frac{\mu_0}{4\,\pi}\,\frac{1}{d^3\,m\,r^2}\sin\beta\,. \tag{4–8}$$

Similarly,

$$-\left(\frac{\mu_0}{8\,\pi}\,\frac{1}{d^3\,m\,r^2} + \frac{1}{m}\,\frac{\mu_0}{2\,\pi}\,\frac{1}{d^5}\right)\cos\beta = -\frac{\mu_0}{8\,\pi}\,\frac{1}{d^3\,m\,r^2}\cos\beta\,. \tag{4–9}$$

Then,

$$\det(B) \approx \frac{1}{m}\,\frac{\mu_0}{\pi}\,\frac{1}{d^4}\,\frac{\mu_0}{8\,\pi}\,\frac{1}{d^3\,m\,r^2} \neq 0\,. \tag{4–10}$$

So, matrix B can be considered as invertible.

Instead of using backstepping design method, filtered tracking error is introduced here,

$$\underline{r} = \underline{\dot{e}} + c\,\underline{e}\,, \tag{4–11}$$

where c is a positive constant.

Open loop analysis of error:

$$\underline{\dot{q}} = \underline{\ddot{q}} - \underline{\ddot{q}}_{des} + c\,\underline{\dot{e}} = B(\underline{q},\ \underline{\dot{q}})\,\underline{u} + G(\underline{q},\ \underline{\dot{q}})c\,\underline{\dot{e}} - \underline{\ddot{q}}_{des} + D\,. \tag{4–12}$$

Design $\underline{u}$ as:

$$\underline{u} = B^{-1}\left(-G - c\,\underline{e} + \underline{\ddot{q}}_{des} - k_1\,\underline{r} - k_2\,\underline{r}\right). \tag{4–13}$$

By such design, since $\underline{r}$ is measureable, $\underline{u}$ is implementable. Also, since $B,\ G,\ D \in \mathcal{L}_\infty$, $\underline{q},\ \underline{q}_{des} \in \mathcal{L}_\infty$ also $\underline{\dot{q}},\ \underline{\dot{q}}_{des} \in \mathcal{L}_\infty$, conclusion $\underline{u} \in \mathcal{L}_\infty$ can be made.

Closed loop analysis of error:

$$\dot{\underline{r}} = \ddot{\underline{q}} - \ddot{\underline{q}}_{des} + c\,\dot{\underline{e}} = -k_1\,\underline{r} - k_2\,\underline{r} + D\,, \tag{4–14}$$

in which, k_1 and k_2 are designed to be positive constant.

For closed loop stability analysis, Lyapunov stability analysis method is used. Let V_L be a continuously differentiable positive definite function defined as:

$$V_L = \frac{1}{2}\,\underline{r}^\top \underline{r}\,. \tag{4–15}$$

Take time derivative of V_L,

$$\dot{V}_L = \frac{1}{2}\,\underline{r}^\top \dot{\underline{r}}\,. \tag{4–16}$$

Substituting we have:

$$\begin{aligned}
\dot{V}_L &= \underline{R}^\top(-k_1\,\underline{r} - k_2\,\underline{r} + D) \\
&= -k_1\,\underline{r}^\top\underline{r} - (k_2\,\underline{r}^\top\underline{r} - \underline{r}^\top D + \frac{1}{4\,k_2}\,D^\top D) + \frac{1}{4\,k_2}\,D^\top D \\
&= -k_1\,\underline{r}^\top\underline{r} - k_2\,(\underline{r} - \frac{1}{2\,k_2}\,D)^\top(\underline{r} - \frac{1}{2\,k_2}\,D) + \frac{1}{4\,k_2}\,D^\top D \\
&\leq -k_1\,V_L + \varepsilon\,,
\end{aligned} \tag{4–17}$$

In which

$$\varepsilon = \frac{1}{4\,k_2}\,D^\top D\,. \tag{4–18}$$

If k_2 can be picked big enough, we can have a very small ε. Consequently,

$$V_L(t) \leq V_L(0)\,e^{-k_1\,t} - \varepsilon\,k_1\,(1 - e^{-k_1\,t})\,. \tag{4–19}$$

Thus, global ultimate bounded result has been proven. The larger k_2 is, the better control performance it demonstrates.

Recall (3–17) and (3–18) in Section 3.4.1

$$
{}^{\delta}\underline{\mu}_A = \begin{bmatrix} \mu_{x\delta} \\ 0 \\ \mu_{z\delta} \end{bmatrix}, \quad \underline{\mu}_B = \mu_{Bx}\,\hat{\underline{x}}_B\,. \tag{4–20}
$$

Actual control input are from three orthogonal rings on satellites A and B, the following equation gives out how to transfer ${}^{\delta}\underline{\mu}_A$ back to body fixed coordinate system:

$$
{}^{A}\underline{\mu}_A = R_{A/R}^{\top}\,{}^{R}\underline{\mu}_A = R_{A/R}^{\top}\,R_{\delta/R}^{\top}\,{}^{\delta}\underline{\mu}_A\,. \tag{4–21}
$$

As well, μ_{Bx} is generated by dominant ring of satellite B.

4.3.1.2 Step 1.A.1 control d and θ_δ

In this step, attitudes of satellite A and B are set to be fixed. Similar to controller design for d and θ_δ, , high gain robust controller for d and θ_δ could be designed. First, reorganize the dynamic equations in the form of $\ddot{\underline{q}} = B(\underline{q},\,\dot{\underline{q}})\,\underline{u} + G(\underline{q},\,\dot{\underline{q}}) + D$,

$$
\underline{q} = \begin{bmatrix} \ddot{\theta}_\delta \\ \ddot{d} \end{bmatrix} = \begin{bmatrix} \frac{1}{m}\,\frac{\mu_0}{2\,\pi}\,\frac{1}{d^5}\cos\beta & \frac{1}{m}\,\frac{\mu_0}{2\,\pi}\,\frac{1}{d^5}\cos\beta \\ -\frac{1}{m}\,\frac{\mu_0}{\pi}\,\frac{1}{d^4}\cos\beta & \frac{1}{m}\,\frac{\mu_0}{2\,\pi}\,\frac{1}{d^4}\sin\beta \end{bmatrix} \begin{bmatrix} u_1 \\ u_2 \end{bmatrix} + \begin{bmatrix} 2\,d\,\dot{\theta}_\delta^2 \\ -\frac{2\,\dot{d}\,\dot{\theta}_\delta^2}{d} \end{bmatrix}. \tag{4–22}
$$

The designed controller has the same form with Step 1.A.0:

$$
\underline{u} = B^{-1}\left(-G - c\,\dot{e} + \ddot{\underline{q}}_{des} - k_1\,\underline{r} - k_2\,\underline{r}\right). \tag{4–23}
$$

Similarity for stability analysis also exists.

4.3.2 Controller for Step 1.B

There is a tricky difference between Step 1.B and Step 1.A. To save control effort, detumbling for $\dot{\theta}_\delta$ will concentrate on driving $\dot{\theta}_\delta$ to zero, thus, after Step 1.A completed, there will be a constant θ_δ stays. However, since during the detumbling process (Step 1.A.1), attitudes of satellite A and B are stabilized by angular momentum, a constant θ_δ will not affect the relationship between $\mathcal{F}^A$, $\mathcal{F}^B$, and $\mathcal{F}^R$.

Due to the high similarity between Step 1.A and Step 1.B, the controller design method for Step 1.B follows the same design process as Step 1.A. Recall the dynamics equations:

$$\ddot{\theta}_\gamma = \frac{1}{m}\frac{\mu_0}{2\,\pi}\frac{\mu_{Ax}}{d^5}\left(\mu_{x\gamma}\cos\alpha + \mu_{z\gamma}\sin\alpha\right) - \frac{2\,\dot{d}\,\dot{\theta}_\gamma}{d}\,, \tag{4–24}$$

$$\ddot{d} = -\frac{1}{m}\frac{\mu_0}{2\,\pi}\frac{\mu_{Ax}}{d^4}\left(2\,\mu_{z\gamma}\cos\alpha - \mu_{x\gamma}\sin\alpha\right) + d\,\dot{\theta}_\gamma^2\,, \tag{4–25}$$

$$\ddot{\alpha} = -\frac{\mu_0}{8\,\pi}\frac{\mu_{Ax}}{d^3\,m\,r^2}\left(2\,\mu_{z\gamma}\sin\alpha + \mu_{x\gamma}\cos\alpha\right) - \frac{1}{m}\frac{\mu_0}{2\,\pi}\frac{\mu_{Ax}}{d^5}\left(\mu_{x\gamma}\cos\alpha + \mu_{z\gamma}\sin\alpha\right) + \frac{2\,\dot{d}\,\dot{\theta}_\gamma}{d}\,. \tag{4–26}$$

4.3.2.1 Step 1.B.0 control d and α

Organize the dynamic equations:

$$\begin{bmatrix}\ddot{d}\\ \ddot{\alpha}\end{bmatrix} = \begin{bmatrix} -\frac{1}{m}\,\frac{\mu_0}{\pi}\,\frac{1}{d^4}\cos\alpha & \frac{1}{m}\,\frac{\mu_0}{2\,\pi}\,\frac{1}{d^4}\sin\alpha \\ -\left(\frac{\mu_0}{4\,\pi}\,\frac{1}{d^3\,m\,r^2} + \frac{1}{m}\,\frac{\mu_0}{2\,\pi}\,\frac{1}{d^5}\right)\sin\alpha & -\left(\frac{\mu_0}{8\,\pi}\,\frac{1}{d^3\,m\,r^2} + \frac{1}{m}\,\frac{\mu_0}{2\,\pi}\,\frac{1}{d^5}\right)\cos\alpha \end{bmatrix}\begin{bmatrix}u_1\\ u_2\end{bmatrix} + \begin{bmatrix} d\,\dot{\theta}_\gamma^2 \\ \frac{2\,\dot{d}\,\dot{\theta}_\gamma}{d}\end{bmatrix} \tag{4–27}$$

where $\underline{u}$ is defined as:

$$\begin{bmatrix}u_1\\ u_2\end{bmatrix} = \begin{bmatrix}\mu_{Ax}\,\mu z\gamma \\ \mu_{Ax}\,\mu x\gamma\end{bmatrix}. \tag{4–28}$$

4.3.2.2 Step 1.B.1 control d and θ_γ

Organize the dynamic equations as:

$$\begin{bmatrix}\ddot{\theta}_\gamma\\ \ddot{d}\end{bmatrix} = \begin{bmatrix} \frac{1}{m}\,\frac{\mu_0}{2\,\pi}\,\frac{1}{d^5}\sin\alpha & \frac{1}{m}\,\frac{\mu_0}{\pi}\,\frac{1}{d^4}\cos\alpha \\ -\frac{1}{m}\,\frac{\mu_0}{2\,\pi}\,\frac{1}{d^4}\cos\alpha & \frac{1}{m}\,\frac{\mu_0}{2\,\pi}\,\frac{1}{d^4}\sin\alpha \end{bmatrix}\begin{bmatrix}u_1\\ u_2\end{bmatrix} + \begin{bmatrix} d\,\dot{\theta}_\gamma^2 \\ -\frac{2\,\dot{d}\,\dot{\theta}_\gamma}{d}\end{bmatrix} \tag{4–29}$$

Then designed input has the same form as in the Step 1.A.1. Refer to Section 3.4.2, transformation of ${}^{\gamma}\underline{\mu}_B$ to body fixed frame $\mathcal{F}^B$, actual input ${}^{B}\underline{\mu}_B$ is given by :

$${}^{\gamma}\underline{\mu}_B = R_{B/R}^{\top}\,R_{\gamma/R}^{\top}\,{}^{\gamma}\underline{\mu}_B\,. \tag{4–30}$$

Also, μ_{Ax} is given by dominant ring of satellite A.

4.3.3 Controller for Step 1.C

Recall the dynamic equation in Section 3.4.3. In this step, a mechanical latch is introduced to keep distance a constant. Thus, the angle difference between y_A and y_B, $(\varphi - \psi)$ is the only one we need to concern.

$$\ddot{d} = \frac{\mu_0\, \mu_{Ay}\, \mu_{By}}{2\, m \pi\, d^4} \cos(\varphi - \psi)\,, \tag{4–31}$$

$$\ddot{\varphi} - \ddot{\psi} = -\frac{\mu_0\, \mu_{Ay}\, \mu_{By}}{4\, \pi\, m\, r^2\, d^3} \sin \varphi - \psi\,. \tag{4–32}$$

Let $q = \varphi - \psi$, $u = \mu_{Ay}\, \mu By$:

$$\ddot{q} = -\frac{\mu_0\, u}{4\, \pi\, m\, r^2\, d^3} \sin q\,. \tag{4–33}$$

Examine the properties mentioned in Section 4.3.1.1, $\sin q$ has singularity when $q = 0,\ pi$. This might cause control input to be unbounded. Thus saturation for input u is necessary. Also, when the initial condition is set to be $q = \pi$, which means y_A and y_B are in the opposite direction, the controller will be invalid. If it is this case, a symmetric mechanical design for docking mechanism could turn $q = \pi$ to be a valid docking attitude.

Controller objective could be expressed as:

$$e = q - q_{des} \to 0\,. \tag{4–34}$$

Following the similar Lyapunov based controller design method, time derivative of filtered error $r = \dot{e} + c\, e$, can be expressed as:

$$\dot{r} = \ddot{q} + c\, \dot{e} = -\frac{\mu_0\, u}{4\, \pi\, m\, r^2\, d^3} \left(\sin q + c\, \dot{e}\right). \tag{4–35}$$

in which c is a positive constant. Design the controller as:

$$u = -\frac{4\, \pi\, m\, r^2\, d^3}{\sin q\, \mu_0} \left(-c\, \dot{e} + \ddot{q}_{des} - k\, \dot{e} - k\, c\, q\right), \tag{4–36}$$

where k is a positive constant.

More discussion about the behavior of this controller will be conducted in simulation section. It is hard to tell if u is bounded, since when $q \rightarrow 0$, $\dot{e}$, $\ddot{q}_{des}$, and $\dot{e} \rightarrow 0$. Information on the converge speeds are needed to verify boundedness of u.

4.3.4 Controller for Step 2

Recall dynamic equation for this step. Notice that, since this step is cooperating with the docking mechanism, while the dynamic model is only for the ideal docking situation, an indicative controller is developed here.

$$\ddot{d} = -\frac{\mu_0}{\pi\, m}\,\frac{\mu_{Ax}\,\mu_{Bx}}{d^4}\,. \tag{4–37}$$

Examine the properties mentioned in Section 4.3.1.1, assume the final d which docking mechanism requires is d_f, then $-\frac{\mu_0}{\pi\, m\, d^4}$ can be considered as bounded and invertible.

Control objective is set to be tracking a desired trajectory d_{des}, then the error is:

$$e = d - d_{des}\,. \tag{4–38}$$

Introducing filtered error:

$$r = \dot{e} + c\,e\,. \tag{4–39}$$

Again, To keep the controller design process concise, replace $\mu_{Ax}\,\mu_{Bx}$ with u, and design control input as:

$$u = -\frac{\pi\, m\, d^4}{\mu_0}\left(-k\,r + \ddot{d}_{des} - c\,\dot{e}\right), \tag{4–40}$$

in which k is chosen to be a positive constant. Closed loop stability analysis has no difference from above controller designs.

4.4 Assumptions for Simulation Parameters

Since this system is designed for docking/proximity operations of small satellites or small assembly parts, all the assumptions for the parameters and limitations are based on common designs for small satellites or micro small satellites. Take CubeSat which is a popular program for small satellites for example [6], the total mass of such a satellites lies in the order of 1 kg, typical size is 0.1 m$\times$0.1 m$\times$0.1 m, power budget

for satellite usually stays a few watts (however, new technology involves the membrane like configuration of solar cells might gives more than 20 W (Watts) power). Note, when satellites are set in docking mode, most of the power will be used for docking mission including actuating the docking process, measuring and controller computing.

Satellites in this thesis are simplified to distribute the mass uniformly to the coils. Based on the above information, satellites mass and coil radius are set as:

$$m = 1 \text{ kg}, \quad r = 0.1 \text{ m}. \tag{4–41}$$

Assumption of 4.5 W budget for driving the electromagnetic coils for each satellite can be fairly made. Then for each coil, 1.5 W is the power limitation. Referring to the design of magnetic torquer in [5] and [8], the power dissipation in one coil can be determined by:

$$P = i^2 R, \tag{4–42}$$

where i is current in coil, and R is resistance of the coil. The coil resistance is given by:

$$R = \frac{2 N \pi r \sigma}{a_w}, \tag{4–43}$$

where N is the number or turns, r is the radius of coil, $\sigma = 1.55 \times 10^{-8}$ Ωm for copper wire, a_w is section area of the coil. For a coil with radius of 0.1 m, a_w $\leq$25 mm^2 is reasonable and suitable for inertial matrix assumption in Chapter 3.

Recall (2–25) magnetic moment of a coil is given by:

$$\mu = N \pi r^2 i = N \pi r^2 \sqrt{\frac{P a_w}{2 N \pi r \sigma}}. \tag{4–44}$$

The larger N is, the larger μ the coil can generate. Thus, a small diameter (d_w) of copper wire with insulation which is available has been chosen to be 0.15 mm. Then $N = \frac{4 a_w}{\pi d_w^2}$ can be approximated.

Substituting, a limitation for the magnetic moment one coil can generate $\mu_{\max} = 73$ Am^2 then can be designed. Additionally, disturbances and noises in simulation will be designed as white noises which have an order of tenth of input forces and torques.

Under these assumptions, simulations for separate steps and several complete simulation result combined with control strategy in different scenarios will be investigated in following sections.

4.5 Simulation and Result

4.5.1 Separate Simulation Result for Each Controller

Before complete simulations for different docking scenarios begin, verification for each controller is essential. Also there are some details about these controller are discussed. Because of the similarity between Step 1.A and Step 1.B, simulations for Step 1.A including Step 1.A.0 and Step 1.A.1 could demonstrate the performance of controllers in both of these two steps.

4.5.1.1 Simulation for Step 1.A.0

Considering the docking strategy, a regulation for d_0 and β_0 to desired constant d_{des} and β_{des} is simulated. A continuous trajectory q_c from initial value q_0 to q_{des} has been designed as such:

$$q_c = q_0 + \frac{(q_{des} - q_0)\,\tanh(\omega\, t - \pi) - \tanh(-\pi)}{1 - \tanh(-\pi)}\,, \tag{4–45}$$

where ω is a positive constant factor adjusting the time the trajectory takes to converge to q_{des}, the larger it is, the faster trajectory converge, the larger control effort it needs.

Recall the flow chart in Figure 4-3 and 4-4 each step needs a criterion to judge whether this step is finished and trig corresponding controller and angular momentum management behavior. For Step 1.A.0, it is set to be $tsA1$. It is defined to be 1 when the following conditions are satisfied: $q - q_{des} \leq 0.01$, $\dot{q} \leq 0.001$ otherwise, it stays 0.

To fully inspect the performance of controller, 3 set of initial conditions have been tested, as shown in Table 4-1.

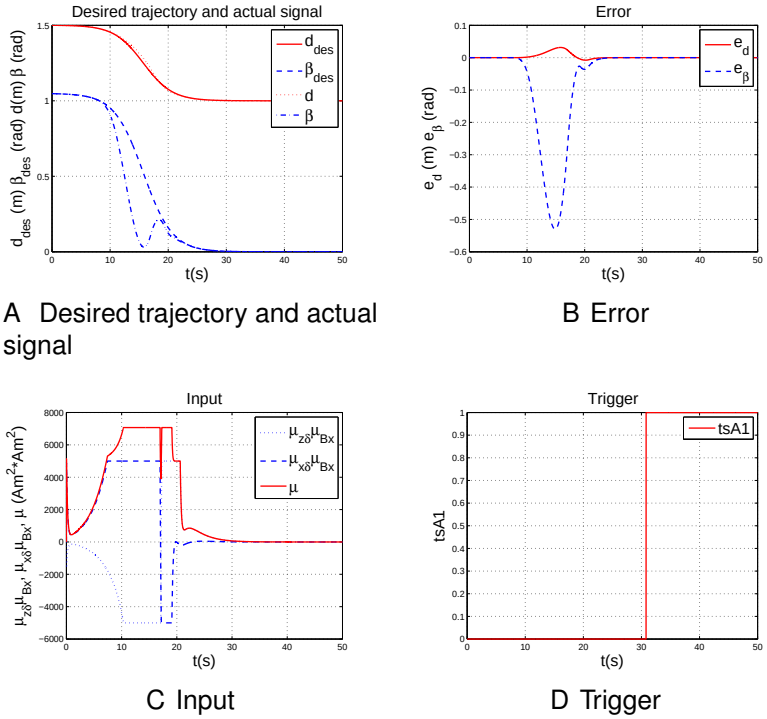

A Desired trajectory and actual signal

B Error

C Input

D Trigger

Figure 4-6. Simulation result for initial condition 1.

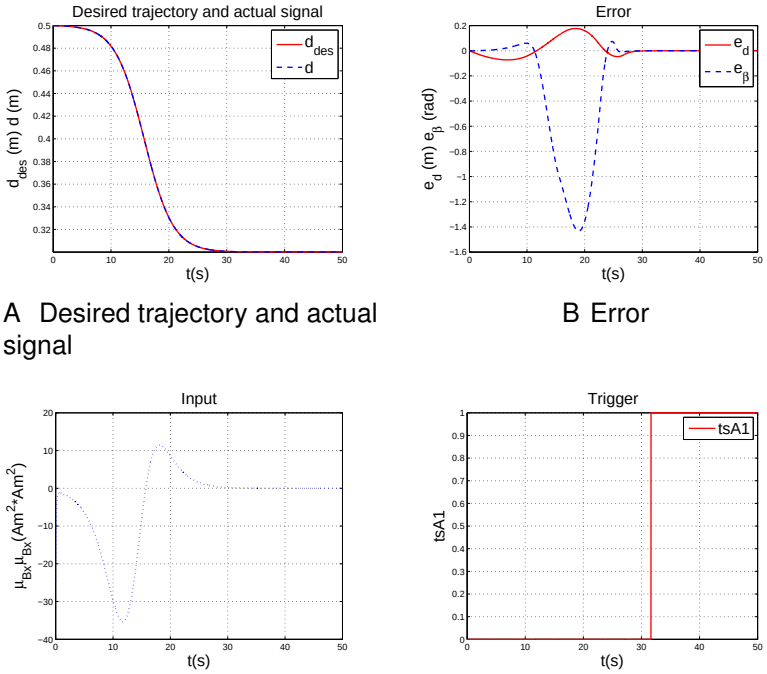

A Desired trajectory and actual signal

B Error

C Input

D Trigger

Figure 4-7. Simulation result for initial condition 2.

Table 4-1. Initial condition for simulation of Step 1.A.0

	d_0 (m)	$\dot{d}_0$ (m/s)	β_0	$\dot{\beta}_0$ (1/s)
1	1.5	0	$\pi/3$	0
2	1.5	0.01	$\pi/2$	-0.02
3	0.8	-0.02	π	0.01

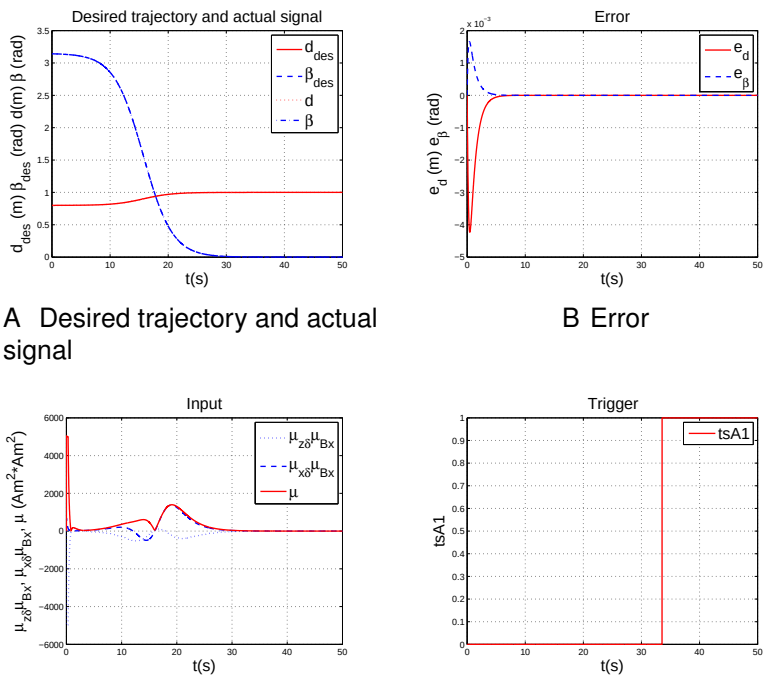

A Desired trajectory and actual signal

B Error

C Input

D Trigger

Figure 4-8. Simulation result for initial condition 3.

Since the docking scenarios are all set to start from attitude stable initial conditions, $\dot{\beta}_0$ is always set to be 0. Also, considering the input limits, $\dot{d}_0$ cannot be large. Actually, for object with dimension of 0.1 m, ± 0.01 m/s is a reasonable assumption. Desired constant d_{des} and β_{des} are set to be 1 m and 0 rad respectively.

Simulation results for these conditions including states variable, error and input, are demonstrated in the following figures: Figure 4-6, Figure 4-7, Figure 4-8. The designed smooth trajectories from d_0 and β_0 to d_{des} and β_{des} have been demonstrated in plot A of each figure. Combining with plot B, presenting the tracking error, and plot C, presenting the inputs, one can draw a conclusion that when control signals stays in the range of input limitations (generally from 0-10 s and 20-30 s), tracking error has a

good performance (under 1×10^3). However, even the saturation affects the tracking errors (generally from 10-20 s), as time goes by, error still can be driven to zero. Trigger indicator tsA1 is turned on about 32 s to 35 s, which means the time consumption for this step is acceptable considering an usual complete docking mission requires $5-10$ minutes [19]. Also the good performance on tracking error indicates that this controller is suitable for the general reasonable initial velocities and angle rates.

4.5.1.2 Simulation for Step 1.A.1

Since, the control objectives in this step are distance regulating or tracking, and detumbling the rotated reference frame, the main control effort should be spent on distance control and detumbling θ_δ ($\dot{\theta}_\delta \rightarrow 0$). When design the trajectory, desired trajectory of θ_δ usually is preferred to drive θ_δ to a constant nearby initial condition $\theta_{\delta 0}$. Without lose of generality, control objective are set to be regulating to $d_{des} = 1$ and $\theta_{\delta des} = \theta_{\delta 0} + \Delta\theta$. In which $\Delta\theta$ is a small angle, again to save control energy, sign of $\Delta\theta$ is defined due to initial rates of $\dot{\theta}_{\delta 0}$. Careful choosing of $\Delta\theta$ will reduce the time to achieve control objective.

In this step, since the attitudes of satellite A and B are set to be stabilized by reaction wheels, β is set to be 0, so is $\dot{\beta}$. Also, due to the trig condition of Step 1.A.1 ($q - q_{des} \leq 0.01$, $\dot{q} \leq 0.001$), initial condition $\dot{d}_0$ is set to be no larger than 0.001, $\dot{\theta}_{\delta 0}$ is the value of $\dot{\theta}_\delta$ when Step 1.A.1 is triggered. Yet to testify the robustness of the controller, the following 2 initial conditions with fairly large $\dot{d}_0$ and $\dot{\theta}_\delta$ shown in Table 4-2 are tested.

Table 4-2. Initial conditions for simulation of Step 1.A.1

	d_0 (m)	$\dot{d}_0$ (m/s)	$\theta_\delta 0$	$\dot{\theta}_{\delta 0}$ (1/s)
1	1.2	-0.01	$\pi/3$	0.02
2	0.8	0.02	$\pi/2$	-0.02

Following the guideline in the beginning paragraph, $\theta_{\delta des} = \pi/3 + \pi/10$ and $\theta_{\delta des} = \pi/2 - \pi/10$. The simulation results for condition 1 and 2 are demonstrated in 2 figures, Figure 4-9 and Figure 4-10. Similar with Step 1.A.0, the tracking error shows a good performance when saturations are not reached (from 10-80 s). Detumbling

a ± 0.02 rad/s level $\dot{\theta}_\delta$ is more time consuming than driving β to zero in Step 1.A.0. Referring to the plot D, trig conditions are usually satisfied at around 90 s. Nevertheless, in a complete simulation, Step 1.A.1 always happens after control objectives of Step 1.A.0 has been achieved which comes usually with a small $\dot{\theta}_\delta$ (about ± 0.005 rad/s). If this is the case, then time consumption will be reduced. More details about this can be reached in complete simulations in Section 4.5.2.

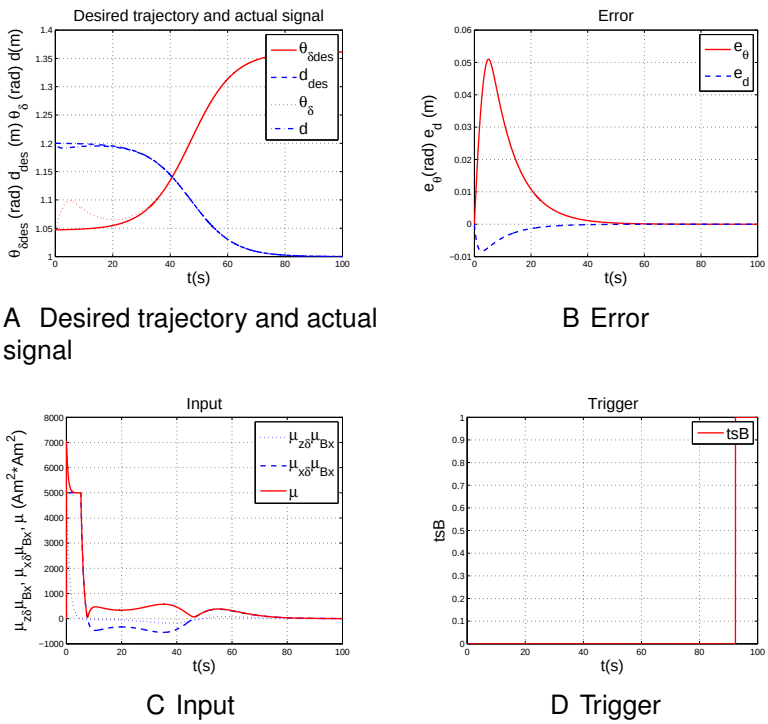

Figure 4-9. Simulation result for Step 1.A.1 in initial condition 1.

4.5.1.3 Simulation for Step 1.C

This step starts with rough docking, which fixed the distance between two satellites. Only twisting angle difference $\varphi - \psi$ will be dealt with in this step. Assume rough docking keeps distance to be $d_r = 0.5$, two sets of initial conditions will be tested for this controller, as shown in Table 4-3. Trigger tsC is defined to be 1 when $\varphi - \psi \leq 0.001$, $\dot{\varphi} - \dot{\psi} \leq 0.001$.

Simulation results for two initial conditions with input saturation are illustrated in Figure 4-11 and 4-12. Trajectory is well followed by observing the plot A and B. As

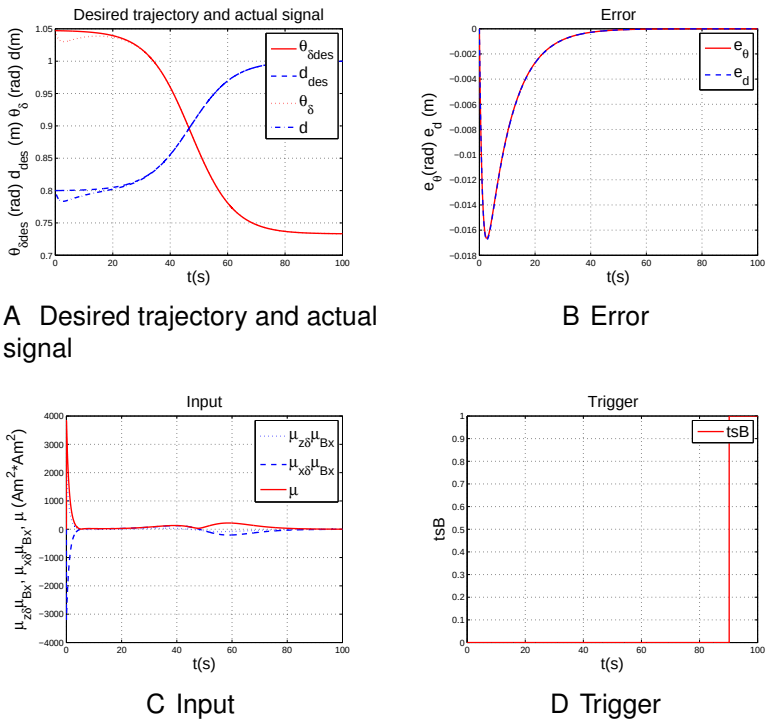

A Desired trajectory and actual signal

B Error

C Input

D Trigger

Figure 4-10. Simulation result for Step 1.A.1 in initial condition 2.

Table 4-3. Initial conditions for simulation of Step 1.C

	$\varphi_0 - \psi_0$ (rad)	$\dot{\varphi}_0 - \dot{\psi}_0$ (1/s)
1	$\pi/2$	-0.01
2	$-\pi/3$	0.02

discussed in the controller design procedure in Section 4.3.3, boundedness of control inputs cannot be guaranteed. Comparing plot A and plot C, singularity of control input happens when y is close to zero. However, as time goes by, one can observe this singularity is an one time accident. After that, the input converges to a constant. And, plot D shows trig indicator ts2 is turned on around 30 s. Comparing with (4–40), throught additional simulations, an unconfirmed conclusion can be inducted that:

$$\lim_{t\to+\infty} u = \frac{4\,k^2\,\pi\,m\,r^2\,d^3}{\mu_0}\,. \tag{4–46}$$

in the two simulations shown, k is chosen to be 0.1, $\lim_{t\to+\infty} u = 12.5$ Am^{2}Am^2. Sum up, saturation for this step is necessary for the singularity issue. To keep the achieved

objective, a constant input is needed. Thus, cooperating with docking mechanism is essential for this step. Also, time consumption is acceptable.

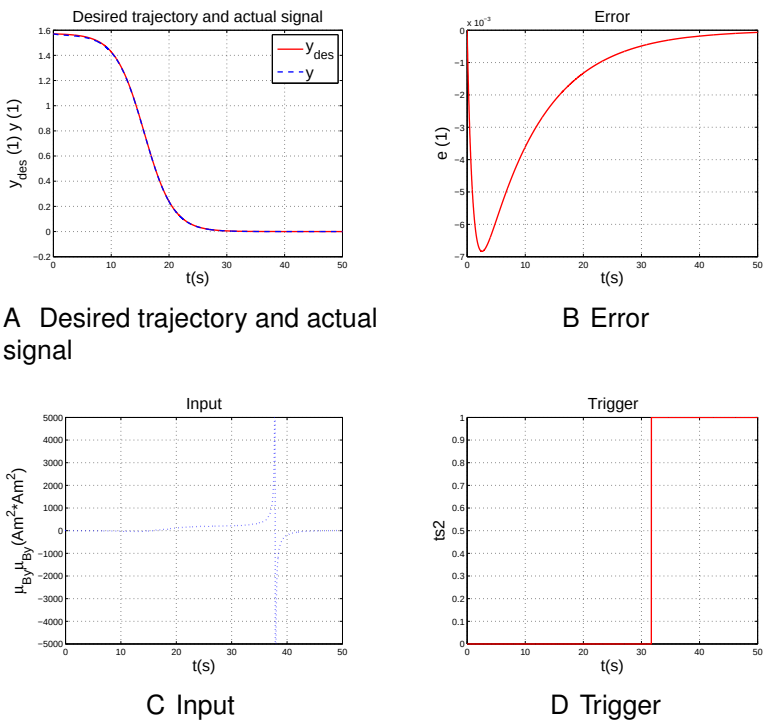

A Desired trajectory and actual signal

B Error

C Input

D Trigger

Figure 4-11. Simulation for Step 1.C in initial condition 1 with saturation.

4.5.1.4 Simulation for Step 2

Initial condition for this step is coming from the rough docking setting. Assume rough docking keeps distance to be $d_r = 0.5$. The actual required distance for mechanical latch is set to be $d_{des} = 0.3$. Simulation result is shown in Figure 4-13. Trigger criterion is satisfied around 25 s. Tracking error in plot B presents a good performance of this controller. Time consumption and energy consumption perform well in this 1-D attraction case.

4.5.2 Complete Simulation

In this section, one complete simulation is demonstrated. Without loss of generality, 2 sets of initial conditions are set as Table 4-4. Except for introducing control algorithm in this section, transforming virtual control inputs for each step to actual currents of rings is also included.

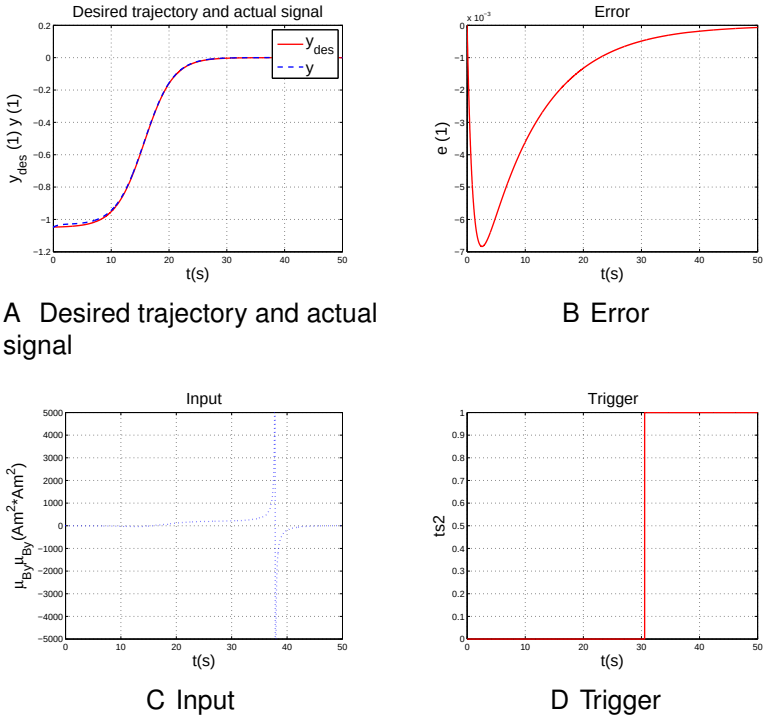

A Desired trajectory and actual signal

B Error

C Input

D Trigger

Figure 4-12. Simulation for Step 1.C in initial condition 2 with saturation.

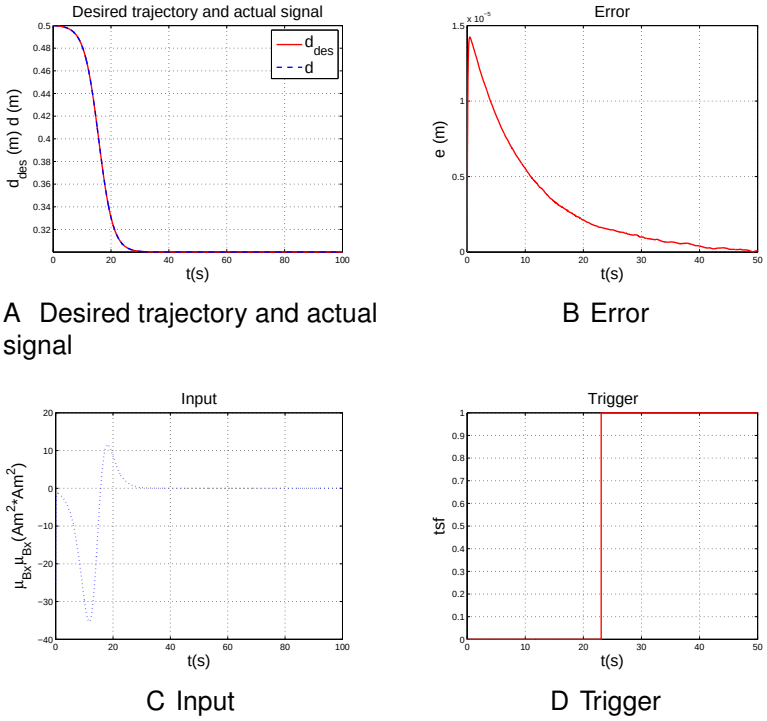

A Desired trajectory and actual signal

B Error

C Input

D Trigger

Figure 4-13. Simulation result for Step 2.

Table 4-4. Initial conditions for complete simulation

	d (m)	$\dot{d}$ (m/s)	α (rad)	β (-)	γ (-)	δ (-)	φ (-)	ψ (-)
1	1.5	0.01	$\frac{\pi}{3}$	$-\frac{3\pi}{4}$	$-\frac{\pi}{4}$	$\frac{\pi}{6}$	$\frac{\pi}{5}$	$-\frac{\pi}{2}$
2	1.7	0.02	$-\frac{\pi}{3}$	π	$-\frac{\pi}{3}$	$-\frac{\pi}{6}$	$\frac{\pi}{4}$	$-\frac{3\pi}{4}$

Observing the virtual control input u for each step, take Step 1.A for example:

$$\underline{u} = \begin{bmatrix} u_1 \\ u_2 \end{bmatrix} = \begin{bmatrix} \mu_{z\delta}\,\mu_{Bx} \\ \mu_{x\delta}\,\mu_{Bx} \end{bmatrix}. \tag{4–47}$$

Calculate the magnitude for input:

$$u = \sqrt{u_1^2 + u_2^2} = \mu_{Bx}\sqrt{\mu_{z\delta}^2 + \mu_{x\delta}^2}\,. \tag{4–48}$$

Assume two satellite has the same power supply ability, then make

$$\mu_{Bx} = \sqrt{\mu_{z\delta}^2 + \mu_{x\delta}^2} = \sqrt{u}\,. \tag{4–49}$$

Thus, magnetic momentum of A represented in $\mathcal{F}^\delta$, ${}^\delta\underline{\mu}_A$, is given by:

$${}^\delta\underline{\mu}_A = \begin{bmatrix} \mu_{x\delta} \\ 0 \\ \mu_{z\delta} \end{bmatrix}. \tag{4–50}$$

Transfer ${}^\delta\underline{\mu}_A$ to $\mathcal{F}^A$,

$${}^A\underline{\mu} = R_{A/R}^\top\,{}^R\underline{\mu}_A = R_{A/R}\,R_{\delta/R}\,{}^\delta\underline{\mu}_A\,. \tag{4–51}$$

Refer to the equations (3–4) and (3–9) for $R_{A/R}$ and $R_{\delta/R}$ in Section 3.2.1 and 3.4.1. It is straightforward to calculate ${}^A\underline{\mu}_A$. Also, μ_{Bx} is generated by dominant ring of B, ${}^B\underline{\mu}_B$ is obviously shown as:

$${}^B\underline{\mu}_B = \begin{bmatrix} \mu_{Bx} \\ 0 \\ 0 \end{bmatrix}. \tag{4–52}$$

The transformations for other steps are similar to this procedure.

The following two set of figures (Figure 4-14 and 4-15 and Figure 4-16 and 4-17) show the d, α, β, and $(\varphi - \psi)$ varies during different steps, and the control inputs (μ_{Ax}, μ_{Bx}, μ_{Ay}, μ_{By}, μ_{Az} and μ_{Bz}) generated by each of the coils which are perpendicular to axes x_A, x_B, y_A, y_B, z_A, and z_B, respectively. Also, five trig indicators for Step 1.A.1, Step 1.B.0, Step 1.B.1, Step 1.C, Step 2 and docking completion (tsA1, tsB, tsB1, tsC, ts2 and tsf) have been demonstrated. Refer to Table 4-5, control objectives and trigger time for each step have been showed.

Table 4-5. Complete simulation result

Step name	Control objective	Trigger time for next step (s)
Step 1.A.0	Regulate d to 1 m, β to 0	tsA1 (32,44 s)
Step 1.A.1	Detumbling θ_δ ($\dot{\theta}_\delta \to 0$), keeping d	tsB (107,118 s)
Step 1.B.0	Regulate d to d_r (0.5 m), α to 0	tsB1 (140,152 s)
Step 1.B.1	Detumbling θ_γ ($\dot{\theta}_\gamma \to 0$), keeping d	tsC (210,188 s)
Step 1.C	Rough docking, regulate $(\varphi - \psi)$ to 0	ts2 (247,226 s)
Step 2	Drive distance to d_{des} (0.3 m)	tsf (270,249 s)

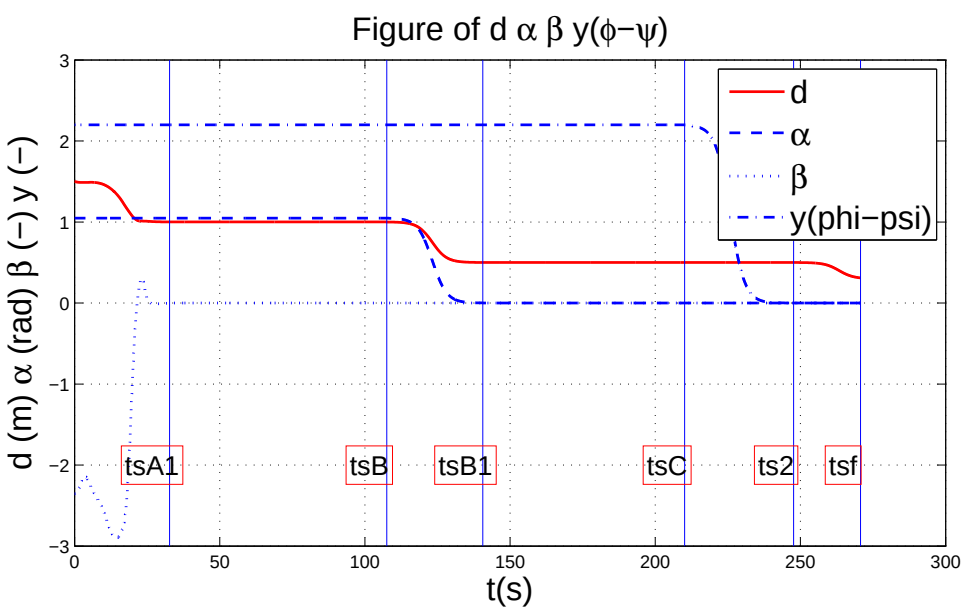

Figure 4-14. Complete simulation for initial condition 1: signal.

To summarize, the controllers for different steps are united together and tested for 2 general different scenarios to demonstrate the effectiveness of the docking and control of two satellites each equipped with 3 orthogonal magnetic coils. The above results

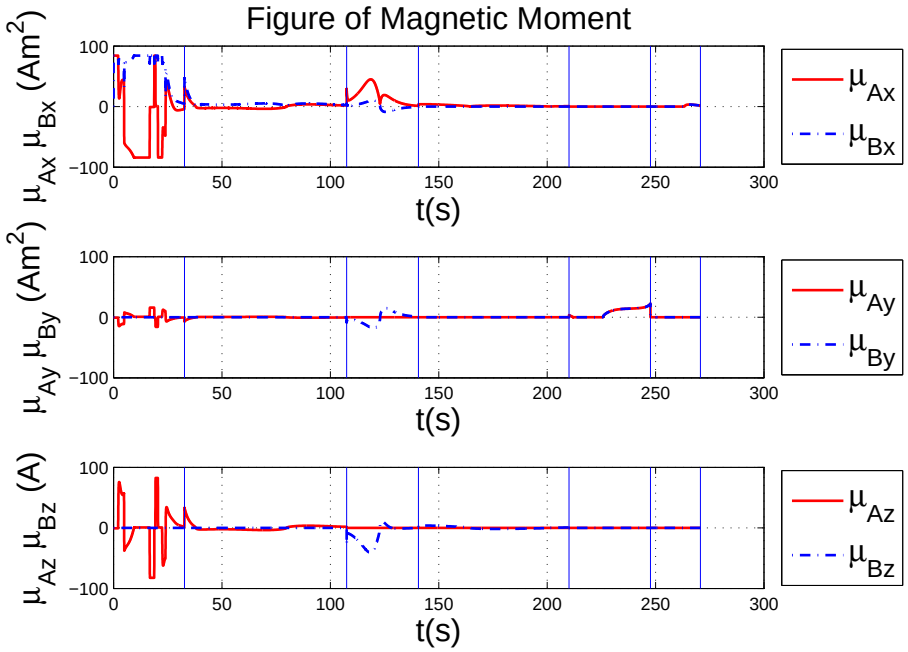

Figure 4-15. Complete simulation for initial condition 1: magnetic moment.

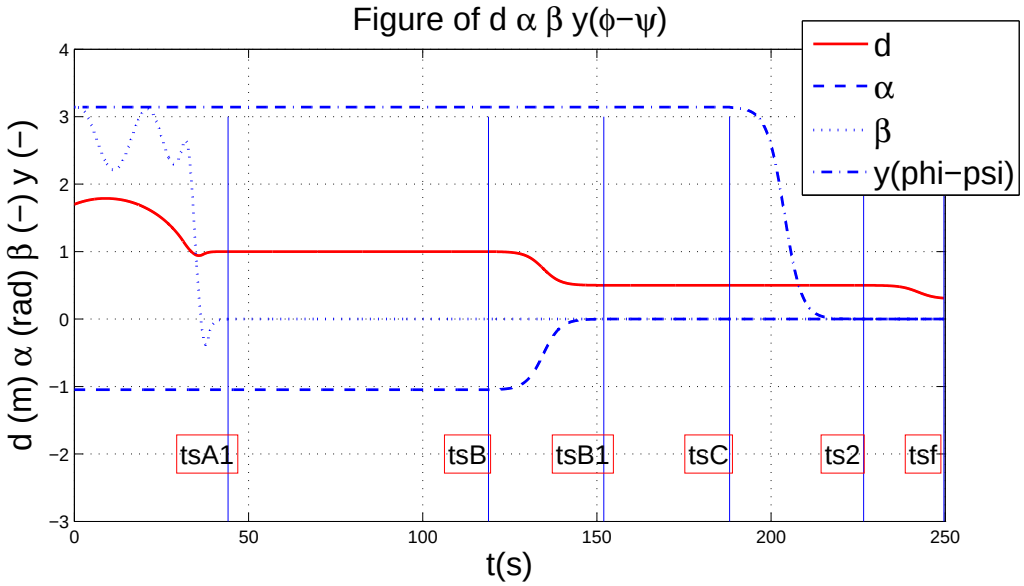

Figure 4-16. Complete simulation for initial condition 2: signal.

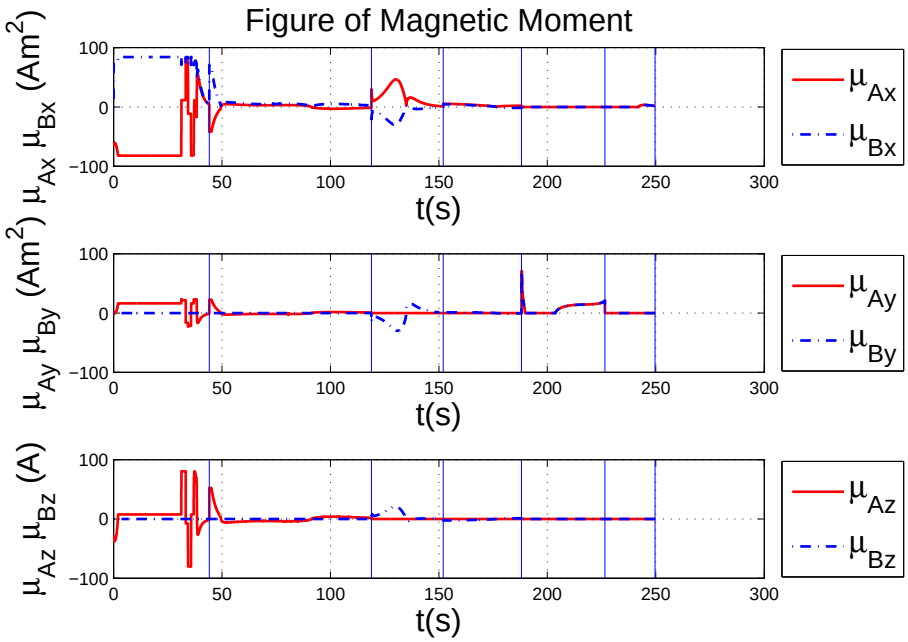

Figure 4-17. Complete simulation for initial condition 2: magnetic moment.

show the whole docking mission costs less than 300s which is the general time with other docking propellent system will cost. Recall Section 4.4, the power requirements for the cases presented match with the input limitation analysis. As well, for each step, disturbances caused by inaccuracy of dynamics model, force and torque generated by uncertainties, and components of forces an torques acting out of the alignment planes or axes have been added to simulation. The robustness of the controllers stays consistent with the results shown in separate simulations in Section 4.5.1. Thus,under deep space assumptions, this docking strategy and control law are applicable for small satellites or assembly parts. In next chapter, more details about expanding this docking strategy to low Earth orbit scenarios will be introduced.

CHAPTER 5
THE LOW EARTH ORBIT CHALLENGES

5.1 Overview

Comparing to deep space assumption, the reality in low earth orbit (LEO) introduces a set of challenges, including the effects of the Earth's gravitational field and magnetic field. In Section 5.2 and 5.3, these two will be addressed. By a simple 2-D case, this chapter presents the dynamics equations in LEO scenario. As well differences from the deep space scenario are demonstrated. Difficulties of solving this problem have been discussed.

5.2 Gravitational Field

When it comes to in orbit case, two types of terms mainly affect the docking dynamics: one is the Earth gravity, another one is orbital angular velocity. Recall Section 3.2.1, the geometry of different coordinate system, when the docking/assembly are operating in some orbit instead of in deep space, $\mathcal{F}^I \neq \mathcal{F}^L$. Consequently, $\underline{\omega}_{L/I} \neq \underline{0}$.

Take dynamics for Step 1.A for example.

$$ {}^{\delta}\underline{\omega}_{\delta/I} = {}^{\delta}\underline{\omega}_{R/L} + {}^{\delta}\underline{\omega}_{L/I} \,, \tag{5–1} $$

$$ {}^{\delta}\underline{P}^{A} = m_A \left({}^{\delta}\dot{\underline{p}}_A + {}^{\delta}\underline{\omega}_{\delta/I} \times {}^{\delta}\underline{P}^{A} \right) = m_A \left({}^{\delta}\dot{\underline{p}}_A + \left({}^{\delta}\underline{\omega}_{R/L} + {}^{\delta}\underline{\omega}_{L/I} \right) \times {}^{\delta}\underline{P}^{A} \right) , \tag{5–2} $$

$$ {}^{\delta}\dot{\underline{P}}^{A} + \left({}^{\delta}\underline{\omega}_{R/L} + {}^{\delta}\underline{\omega}_{L/I} \right) \times {}^{\delta}\underline{P}_A = {}^{\delta}\underline{F}_A \,, \tag{5–3} $$

in which ${}^{\delta}\underline{F}_A$ include both electromagnetic force and gravity force. Similar changes will happen to rotational dynamics.

For describing the orbital relative position/attitude problem, when the Earth is modeled as a perfect sphere, Clohessy-Wiltshire (CW) or Hill's equations are usually

used [18]. Since CW equations are expressed in the local in orbit frame $\mathcal{F}^L$ as following,

$$ {}^L\ddot{x} + n^2\,{}^Lx = \frac{{}^LF_x}{m}\,, \tag{5–4} $$

$$ {}^L\ddot{y} - 3\,n^2\,{}^Ly - 2\,n\,{}^L\dot{z} = \frac{{}^LF_y}{m}\,, \tag{5–5} $$

$$ {}^L\ddot{z} + 2\,n\,{}^Ly = \frac{{}^LF_z}{m}\,, \tag{5–6} $$

where ${}^LF$ is the force act on this object except gravity, n is the orbital frequency, given by:

$$ n = \sqrt{\frac{\mu_e}{r_e^3}}\,, \tag{5–7} $$

where the gravitational constant of Earth $\mu_e = 3.98 \times 10^5$ km^3/s^2, r_e is the orbital radius of these two satellites' center of mass.

When studying in orbit case, translational dynamics model is preferred to be derived in $\mathcal{F}^L$. The complexity of transfer matrix and states variable estimation in 3-D reality is not helpful for demonstrating how orbit case should be derived. Thus, a simple new 2-D case as shown in Figure 5-1 is presented in this section.

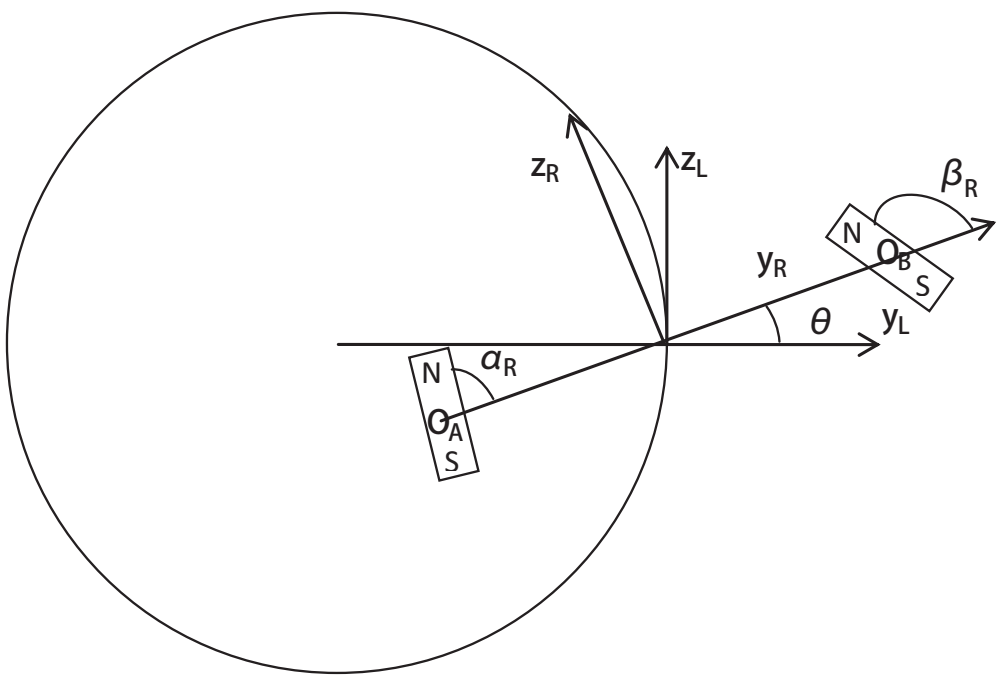

Figure 5-1. A 2-D case concerns orbital dynamics.

Assume dipole A and B are generated by ring A and B, which has the identical size and mass. In this case, by using CW (5–6), translational dynamics equations are derived as:

$$ {}^{L}\ddot{y}_A - 3\,n^2\,{}^{L}y_A - 2\,n\,{}^{L}\dot{z}_A = \frac{{}^{L}F_y}{m}\,, \tag{5–8} $$

$$ {}^{L}\ddot{z}_A + 2\,n\,{}^{L}y_A - 2\,n\,{}^{L}\dot{z}_A = \frac{{}^{L}F_z}{m}\,. \tag{5–9} $$

Position of O_A represented in $\mathcal{F}^L$ is $({}^{L}y_A,\ {}^{L}z_A)$, m is the mass of ring A, and

$$ \begin{bmatrix} {}^{L}F_y \\ {}^{L}F_z \end{bmatrix} = \begin{bmatrix} \cos\theta & \sin\theta \\ -\sin\theta & \cos\theta \end{bmatrix} \begin{bmatrix} {}^{R}F_{Ay} \\ {}^{R}F_{Az} \end{bmatrix}. \tag{5–10} $$

where

$$ \cos\theta = \frac{{}^{L}y_A}{\sqrt{{}^{L}y_A^2 + {}^{L}z_A^2}}\,, \sin\theta = \frac{{}^{L}z_A}{\sqrt{{}^{L}y_A^2 + {}^{L}z_A^2}}\,. \tag{5–11} $$

Recall expressions for electromagnetic force in Section 2.3.2,

$$ \begin{bmatrix} {}^{R}F_{Ay} \\ {}^{R}F_{Az} \end{bmatrix} = \frac{3\,\mu_0}{4\,\pi}\,\frac{\mu_A\,\mu_B}{d^4} \begin{bmatrix} 2\cos\alpha_R\cos\beta_R - \sin\alpha_R\sin\beta_R \\ -\cos\alpha_R\sin\beta_R - \cos\beta_R\sin\alpha_R \end{bmatrix}, \tag{5–12} $$

where $d = 2\sqrt{{}^{L}y_A^2 + {}^{L}z_A^2}$.

The rotational dynamics equation can be easily derived since this is a coplanar case:

$$ I_x(\ddot{\alpha}_R + \ddot{\theta}) = -\frac{\mu_0}{4\,\pi}\,\frac{\mu_A\,\mu_B}{d^3}\,(2\sin\alpha_R\cos\beta_R + \cos\alpha_R\sin\beta_R)\,, \tag{5–13} $$

$$ I_y(\ddot{\beta}_R + \ddot{\theta}) = -\frac{\mu_0}{4\,\pi}\,\frac{\mu_A\,\mu_B}{d^3}\,(2\cos\alpha_R\sin\beta_R + \sin\alpha_R\cos\beta_R)\,, \tag{5–14} $$

where I_x is the x component of inertia of ring A/B.

Observing the dynamics equations, θ and d no longer stay in dynamics equations explicitly. Either control objective needs to be transformed or the dynamic equation should. It depends on the actual sensors and states estimation method. Especially, when it comes to 3-D, the transforming becomes more difficult. However, the docking

strategy and controller design method shown in Chapter 4 still works. Besides, when the orbit period is long enough comparing to the consumed time on docking, the influence of orbit dynamics could be considered as disturbances. Based on more knowledge on states estimation, considering about orbit dynamics will become easier. In future work, this part is highly recommended.

5.3 Geomagnetic Field

When this system is operating in Earth's magnetic field, the electromagnetic coils produce force and torque on the satellites. Force generated by geomagnetic field is a function of the gradient of the local magnetic field[15]:

$$\underline{F}_{GM} = \nabla B_E \, \underline{\mu} \,, \tag{5–15}$$

where B_E is the magnitude of local magnetic field, $\underline{\mu}$ is a dipole moment generated by the coil.

Torque generated by geomagnetic field is given by:

$$\underline{\tau}_{GM} = \underline{\mu} \times \underline{B}_E \,. \tag{5–16}$$

By examining and the qualitative analysis [15], the amount of disturbance force produced on satellite due to geomagnetic field is less than tenths of a percent of the interacting forces between two satellites. However, the torque is on the same order of interacting torque. So when geomagnetic field is considered, the disturbance force is negligible, while the torque must be taken into account.

Take the simple example in Section 5.2 for example, considering the small size of coils, the direction and magnitude of $\underline{B}_E$ are assumed fixed, presented in Figure 5-2. The torque produced by geomagnetic field can be calculated:

$$^{L}\underline{\tau}_{AG} = {}^{L}\underline{\mu}_A \times {}^{L}\underline{B}_E = \mu_A \left(\cos\alpha_R \, B_{Ez} - \sin\alpha_R \, B_{Ey}\right) , \tag{5–17}$$

$$^{L}\underline{\tau}_{BG} = {}^{L}\underline{\mu}_B \times {}^{L}\underline{B}_E = \mu_B \left(\cos\beta_R \, B_{Ez} - \sin\beta_R \, B_{Ey}\right) , \tag{5–18}$$

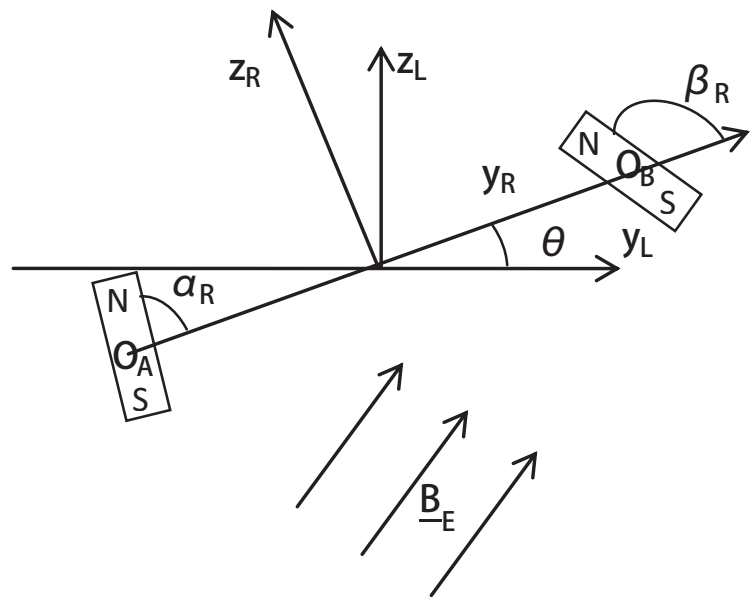

Figure 5-2. A simple 2-D case concerns geomagnetic field.

The rotational dynamics equations become:

$$Ix\left(\ddot{\alpha}_R+\ddot{\theta}\right)=-\frac{\mu_0}{4\,\pi}\,\frac{\mu_A\,\mu_B}{d^3}\left(2\sin\alpha_R\cos\beta_R+\cos\alpha_R\sin\beta_R\right)+\mu_A\left(\cos\alpha_R\,B_{Ez}-\sin\alpha_R\,B_{Ey}\right), \tag{5–19}$$

$$Iy\left(\ddot{\beta}_R+\ddot{\theta}\right)=-\frac{\mu_0}{4\,\pi}\,\frac{\mu_A\,\mu_B}{d^3}\left(2\cos\alpha_R\sin\beta_R+\sin\alpha_R\cos\beta_R\right)+\mu_B\left(\cos\beta_R\,B_{Ez}-\sin\beta_R\,B_{Ey}\right). \tag{5–20}$$

The similar docking strategy can be transplanted to this case. First step, set attitude of A fixed, regulate β_R to zero. Then set B fixed, regulate α_R to zero. Consider both of the two dipoles are steerable, which means any direction and magnitude of the magnetic moment can be generated. Take the first step for example, reorganize it as:

$$Ix\left(\ddot{\alpha}_R+\ddot{\theta}\right)=-\frac{\mu_0}{4\,\pi}\,\frac{\mu_A}{d^3}\left(2\sin\alpha_R\,\mu_{By}+\cos\alpha_R\,\mu_{Bz}\right)+\mu_A\left(\cos\alpha_R\,B_{Ez}-\sin\alpha_R\,B_{Ey}\right), \tag{5–21}$$

in which $\mu_{By}=\mu_B\cos\beta_R$, $\mu_{Bz}=\mu_B\sin\beta_R$.

It is interesting that there are 3 inputs (μ_A, μ_{By} and μ_{Bz}). Recall the control objective for Step 1.A in Section 4.3.1: controlling β is for the purpose of aligning B's dominant axis with distance vector, controlling d gives the ability of regulating the distance or

tracking a desired trajectory, controlling θ_δ is for detumbling the rotated reference coordinate system $\mathcal{F}^R$. The dynamic equation shows 3 degrees of freedom.

Separating Step 1.A to two steps is trying to avoid the problem of lacking control input. After introducing geomagnetic, all the 3 control objectives can be done in one controller. This could also be a part of future work.

CHAPTER 6
CONCLUSION

6.1 Summary of the Thesis

This thesis starts from the idea that using electromagnetic force and torque to adjust the relative positions and attitudes in docking/assembly and other proximity operations. Based on some careful assumptions, this thesis investigates a capable docking strategy to achieve this goal. The key objectives of this thesis were to present this electromagnetic docking idea is feasible from the dynamics and control point of view.

In the following paragraphs, the chapter-wise summary of this thesis are demonstrated:

Chapter 1 introduces the basic idea of electromagnetic docking and shows the advantages over conventional propulsion. Also, previous relative works and the differences from other researches have been provided.

Chapter 2 uses the principle of magnetic field theory, describes the applicable theory of magnetic field model for this thesis. Exact model has been presented firstly, and then linearization of this model leads to a far field model. Base on this far field model, force and torque equations for several principal basic configurations of coils have been derived.

Chapter 3 describes the system and the overall docking strategy with deep space assumption. Decoupling 3-D problem to several steps of principal basic cases including 2-D co-planar case, co-axial twist case and 1-D distance control case. Then development of dynamic models for each of these cases has been investigated.

Chapter 4 demonstrates the overall control strategy which accommodates with the docking strategy. Then, the controller design and simulation results of each step have been presented. As well, a complete docking procedure simulation has been performed.

Chapter 5 states the difficulties when this system is operating in low earth orbit. Based on a simple 2-D case, this chapter presents how the gravitational field and

geomagnetic field affect this system. After discussion about the dynamic of this simple case, suggestions for future work directions have been given.

This thesis starts a new thinking of introducing electromagnetic forces and torques to docking/assembly and proximity operations missions, which is combining the translational and rotational degrees of freedom together and designing control law for them. Other presented works usually decoupled them to two independent problem by cooperating with a complete attitude control system. Though, this approach is straightforward to think, it also loses the insight about the behaviours of electromagnetic forces and torques, about how they are coupled with the relative position and attitude.

By a series of simulations, the docking strategy in this thesis has been proven to be feasible and robust for multi-scenarios. Also, power consumption and time cost have been demonstrated suitable for small space vehicles.

6.2 Future Work

This thesis concentrates on the conception of electromagnetic docking/assembly and proximity operation system from the basic dynamics and control point of view. Thus necessary assumptions about the work scenario, implement methods and equipments have been made. Several recommendations are given for future work:

The input saturation influences the controller performance heavily. Controller design with saturation compensator is a good direction to improve the performance.

Combining with states estimation research, in orbit case can be investigated more deep.

Based on the idea introduced in Chapter 5 about how to exploit geomagnetic field for this system, 3-D expansion could be part of the future work.

APPENDIX A
MATRIX NORM

A matrix norm is a natural extension of the notion of a vector norm to matrices [3], [21]. The p-norm for a $n \times m$ matrix A is defined as:

$$\|A\|_p = \max_{x \neq 0} \frac{\|A\,x\|_p}{\|x\|_p} \,. \tag{A–1}$$

In the case of $p = 1$, the norm can be computed as:

$$\|A\|_1 = \max_{1 \leq j \leq n} \sum_{i=1}^{m} |a_{ij}| \,, \tag{A–2}$$

which is simply the maximum absolute column sum of the matrix A.

In case of $p = \infty$ the norms can be computed as:

$$\|A\|_\infty = \max_{1 \leq j \leq m} \sum_{j=1}^{n} |a_{ij}| \,, \tag{A–3}$$

which is the maximum absolute row sum of the matrix A.

The 2-norm is the one, usually used in bounding a matrix. There is an inequalities relationship among $\|A\|_2$ and $\|A\|_1$ and $\|A\|_\infty$:

$$\frac{1}{\sqrt{n}}\|A\|_\infty \leq \|A\|_2 \leq \sqrt{m}\|A\|_\infty \,, \tag{A–4}$$

$$\frac{1}{\sqrt{m}}\|A\|_1 \leq \|A\|_2 \leq \sqrt{n}\|A\|_1 \,. \tag{A–5}$$

So, proving matrix A is bounded, is equivalent to proving every absolute column sum of the matrix A is bounded. It is sufficient to have every absolute element of matrix A be bounded.

REFERENCES

[1] Ahsun, U. *Dynamics and control of electromagnetic satellite formations*. Ph.D. thesis, Massachusetts Institute of Technology. Dept. of Aeronautics and Astronautics., 2007.

[2] Camillo, P. J. and Markley, F. L. "Orbit-averaged behavior of magnetic control laws for momentum unloading." *Journal of Guidance and Control* 3 (1980): 563–568.

[3] Demmel, J. W. *Applied Numerical Linear Algebra*. SIAM, 1997.

[4] Dennison, E. "Off-Axis Field Due to a Current Loop." 2005.

URL http://www.netdenizen.com/emagnet/offaxis/iloopoffaxis.htm

[5] Graversen, T., Frederiksen, M. K., and Vedstesen, S. V. *Attitude Control system for AAU CubeSat*. Master's thesis, Aalborg University, 2002.

[6] Hank, H., Jordi, P.S., Augustus, S. M., Schinichi, N., and Robert, J. T. "CubeSat: A new Generation of Picosatellite for Education and Industry Low-Cost Space Experimentation." *14th Annual/USU Conference on Small Satellites* 5 (2000).

[7] Hughes, P. C. *Spacecraft Attitude Dynamics*. Dover Publications, 2004.

[8] Jens, G. *Development of an Active Magnetic Attitude Determination and Control System for Picosatellites on highly inclined circular Low Earth Orbits*. Master's thesis, School of Aerospace, Mechanical and Manufacturing Engineering, Science, Engineering and Technology Portfolio, RMIT University, 2006.

[9] Kaneda, R., Yazaki, F., Sakai, S., Hashimoto, T., and Saito, H. "The Relative Position Contro in Formation Flying Satellites using Super-Conducting Magnets." *2nd International Symposium on Formation Flying Missions and Technologies*. 2004.

[10] Khalil, H. K. *Nonlinear Systems*. Prentice Hall, Inc., 2002, 3rd ed.

[11] Lee, D-R and Pernicka, H. "Optimal Control for Proximity Operations and Docking." *International Journal of Aeronautical and Space Sciences* 11 (2010).3: 206–220.

[12] M.Patre, P., MacKunis, W., Dupree, K., and Dixon, W. E. "A new class of modular adaptive controllers, Part I: Systems with linear-in-the-parameters uncertainty." *American Control Conference* (2008): 1208 –1213.

[13] Pollack, G. L. and Stump, D. R. *Electromagnetism*. Addison Wesley, 2002.

[14] Reynerson, C.M. "Spacecraft modular architecture design for on-orbit servicing." *IEEE Aerospace Conference Proceedings* 4 (2000): 227– 238.

[15] Schweighart, S. A. *Electromagnetic formation flight dipole solution planning*. Ph.D. thesis, Massachusetts Institute of Technology, Dept. of Aeronautics and Astronautics, 2005.

[16] Silani, E. and Lovera, M. "Magnetic spacecraft attitude control: a survey and some new results." *Control Engineering Practice* 13 (2005): 357C371.

[17] Sofyali, A. and Aslan, A. R. "Magnetic attitude control of small satellites: a survey of applications and a domestic example." Tech. rep., Istanbul Technical University, Space Systems Design and Testing Laboratuary, 2011.

[18] Steve, N. "ASEN 5050 Spaceflight Dynamics." 2011.

URL http://ccar.colorado.edu/asen5050/ASEN5050/Lectures_files/lecture11.pdf

[19] Werts, J. R. and Bell, R. "Autonomous Rendezvous and Docking Technologies - Status and Prospects." *Proceedings of SPIE AeroSense Symposium* 5088 (2003): 20.

[20] Wiens, G. J. and Maldonado, L. "Autonomous Torque-Actuated Foldable Docking Mechanism for Small Space Vehicles." *2011 Florida Conference on Recent Advances in Robotics* 1 (2011): 200–209.

[21] Wikipedia, the free encyclopedia. "Matrix norm." 2010.

URL http://en.wikipedia.org/wiki/Matrix_norm

[22] Zhang, Y.W., Yang, L.P., Zhu, Y.W., Ren, X.H., and Huang, H. "Self-docking capability and control strategy of electromagnetic docking technology." *Acta Astronautica* 69 (2011): 1073C1081.

[23] ———. "Nonlinear 6-DOF control of spacecraft docking with inter-satellite electromagnetic force." *Acta Astronautica* 77 (2012): 97–108.

BIOGRAPHICAL SKETCH

Ke Huo received his Bachelor of Science in Aerospace Engineering from the Beihang University, China, in 2009, Master of Science in Aerospace Engineering from the University of Florida in 2012.